SMAI-JCM
SMAI Journal of Computational Mathematics

Compatible Maxwell solvers with particles I: conforming and non-conforming 2D schemes with a strong Ampere law

Martin Campos Pinto & Eric Sonnendrücker

Volume 3 (2017), p. 53-89.

<http://smai-jcm.cedram.org/item?id=SMAI-JCM_2017__3__53_0>

SMAI Journal of Computational Mathematics
Vol. 3, 53-89 (2017)

Compatible Maxwell solvers with particles I: conforming and non-conforming 2D schemes with a strong Ampere law

Martin Campos Pinto [1]
Eric Sonnendrücker [2]

[1] CNRS, Sorbonne Universités, UPMC Univ Paris 06, UMR 7598, Laboratoire Jacques-Louis Lions, 4, place Jussieu 75005, Paris, France
E-mail address: campos@ljll.math.upmc.fr
[2] Max-Planck Institute for plasma physics, Boltzmannstr. 2, D-85748 Garching, Germany, Mathematics Center, TU Munich, Boltzmannstr. 3, D-85747 Garching, Germany
E-mail address: sonnen@ipp.mpg.de.

Abstract. This article is the first of a series where we develop and analyze structure-preserving finite element discretizations for the time-dependent 2D Maxwell system with long-time stability properties, and propose a charge-conserving deposition scheme to extend the stability properties in the case where the current source is provided by a particle method. The schemes proposed here derive from a previous study where a generalized commuting diagram was identified as an abstract compatibility criterion in the design of stable schemes for the Maxwell system alone, and applied to build a series of conforming and non-conforming schemes in the 3D case. Here the theory is extended to account for approximate sources, and specific charge-conserving schemes are provided for the 2D case. In this article we study two schemes which include a strong discretization of the Ampere law. The first one is based on a standard conforming mixed finite element discretization and the long-time stability is ensured by a Raviart-Thomas finite element interpolation for the current source, thanks to its commuting diagram properties. The second one is a new non-conforming variant where the numerical fields are sought in fully discontinuous spaces. Numerical experiments involving Maxwell and Maxwell-Vlasov problems are then provided to validate the stability of the proposed methods.

Math. classification. 35Q61, 65M12, 65M60, 65M75.

Keywords. Maxwell equations, Gauss laws, structure-preserving, PIC, charge-conserving current deposition, conforming finite elements, discontinuous Galerkin, Conga method.

1. Introduction

As is well known, the issue of long-time stability in time-dependent Maxwell solvers is strongly related to the good preservation of the divergence constraints at the discrete level. More precisely, numerical approximations to the Faraday and Ampère equations

$$\begin{cases} \partial_t \boldsymbol{B} + \mathbf{curl}\, \boldsymbol{E} = 0 \\ \partial_t \boldsymbol{E} - c^2\, \mathbf{curl}\, \boldsymbol{B} = -\dfrac{1}{\varepsilon_0} \boldsymbol{J} \end{cases}$$

should preserve some proper versions of the Gauss laws

$$\begin{cases} \operatorname{div} \boldsymbol{E} = \dfrac{1}{\varepsilon_0} \rho \\ \operatorname{div} \boldsymbol{B} = 0 \end{cases}$$

as is the case for the exact solutions. Indeed when they fail to do so, small errors are observed which often accumulate into large deviations unless some dissipative processes are added to the simulation. In a recent work [22], we have found that a generalized commuting diagram expressing a compatibility property with respect to the Gauss laws could be used as a key criterion to guarantee the long-time

stability of the approximate fields, and this criterion has then been applied to design conforming and non-conforming Gauss-compatible solvers for the 3D Maxwell system.

Our work follows a vast literature aiming at understanding the key structures that are needed at the discrete level for a good approximation of Maxwell's equations in different settings as only the Yee method [73] on staggered grids was able to achieve for a long time. Discretization techniques based on an interpretation of Maxwell's equations based on differential forms were pioneered by Bossavit [10, 11] and further developped by Hiptmair [39, 40, 41] who proposed a unifying framework for the construction and analysis of conforming Finite Elements discretizations. After that, many authors have underlined the central role of the de Rham diagram and its discrete version for the successful derivation of solvers based on conforming Finite Elements, for time dependent solvers [71, 64, 72, 75] as well as for the eigenvalue problem [6, 7, 56], where it proved crucial in order to prove convergence. There also is a large amount of work on the numerical analysis of the commuting diagram involving the projections from the continuous de Rham diagram to its discrete counterpart [27, 28]. The main results concerning the curl-conforming Finite Element approximation of the time-dependent problem can be found in the articles of Monk [52, 53, 54]. An extensive study of the time-harmonic problem can be found in his book [55] which also reviews most functional analysis tools for the time-dependent problem, for which [23] and [49] are important references. We also mention Joly [45] who pinpoints the importance of a formally adjoint structure similar to ours, and [14] for a very interesting discrete de Rham sequence based on B-splines. The general theory of Finite Element Exterior Calculus (FEEC) for general applications including Maxwell was presented by Arnold, Falk and Whinter in [4]. As a key tool in this analysis, we should also mention the works on smoothed polynomial projections [24, 65, 2, 25, 33], which allow to establish the stability of the associated finite element discretizations. This is the context in which our work, starting in [22], should be placed. It underpins the structure which is needed for the compatibility of the dynamical Maxwell equations with the divergence constraints. This structure is already available in conforming Finite Elements based on a discrete De Rham sequence, but fully understanding it permits us to design compatible schemes involving non-conforming Finite Element spaces, such as fully discontinuous ones. This represents an interesting alternative to existing Discontinuous Galerkin schemes for Maxwell's equations [37, 38, 34, 13], indeed our non-conforming schemes do not require dissipative or divergence cleaning techniques for long-time stability or spectral correctness.

In the present work we extend our previous study [22] in two directions. On a theoretical level first, we propose a stability analysis that allows to handle the case where the Maxwell discretization is coupled with another numerical solver for the current $\boldsymbol{J}$, such as a current obtained from a Vlasov equation

$$\partial_t f + \boldsymbol{v} \cdot \boldsymbol{\nabla}_{\boldsymbol{x}} f + \frac{q}{m}(\boldsymbol{E} + \boldsymbol{v} \times B) \cdot \boldsymbol{\nabla}_{\boldsymbol{v}} f = 0 \tag{1.1}$$

describing the collisionless evolution of one or several particle species with charge q and mass m, through their distribution function $f = f(t, \boldsymbol{x}, \boldsymbol{v})$. Here the current density needed in Maxwell's equations is defined from the particle distribution f as $\boldsymbol{J} := q \int \boldsymbol{v} f \, \mathrm{d}\boldsymbol{v}$ and the charge density appearing in the Gauss law is $\rho := \int f \, \mathrm{d}\boldsymbol{v}$. Because the theoretical stability properties of Gauss-compatible schemes rely on the ability to approximate the exact source with a well-designed approximation operator, they are not readily applicable in the case of approximate sources. One must then make an explicit use of the Gauss laws to derive long-time stability estimates. The exact preservation of a proper discrete Gauss law then leads us to an additional criterion to couple the approximate current with the Maxwell discretization, which is formulated as a discrete version of the continuity equation

$$\partial_t \rho + \operatorname{div} \boldsymbol{J} = 0$$

since this is the relation that guarantees the preservation of the Gauss laws for the exact solutions to the Faraday and Ampère equations.

This approach follows the classical principles of charge-conserving deposition schemes that have been developped in computational physics for several decades [30, 70, 32], so that our contribution can be seen as a rigorous generalization of this approach to general discretizations. In particular, we show that an abstract class of structure-preserving discretizations characterized by exact sequences of uniformly stable operators yields long-time stability properties for the discrete fields. An important point is that our criterion involves not only the discrete curl operators corresponding to the approximation of the time-dependent Maxwell equations but also the discrete divergence operators corresponding to the Gauss laws. As a consequence, this framework allows us to characterize *proper discrete continuity equations* that should be satisfied by the approximate sources. This on the one hand provides a rigorous analysis explaining why conforming Finite Element methods based on a de Rham diagram naturally provide a stable coupling with discrete Vlasov solvers. On the other hand it provides a convenient framework to define a stable, charge-conserving coupling for non-conforming Finite Element methods.

This is to our knowledge the first rigorous analysis of stable particle coupling for generic Maxwell solvers with particles, which has been an ongoing problem since the first days of electromagnetic Particle in Cell (PIC) simulations. The first remedies have been to correct the electric field by solving exact [9] or approximate [51, 47] Poisson equations, until Eastwood, Villasenor and Buneman [30, 70] noticed that stable solvers could be obtained by an adequate computation of the current from the particles which would preserve a discrete Gauss law. In the framework of curl-conforming finite element method, we have described a generic algorithm in [17], revisited in a geometric perspective in [66, 57]. More recently it was noticed that this algorithm fits in a semi-discrete Hamiltonian structure, where the divergence constraints are identified as Casimirs and thus are automatically conserved [46]. For non-conforming Maxwell solvers such as Discontinuous Galerkin (DG) solvers, most numerical methods rely on divergence cleaning techniques [59, 58, 43, 44, 68, 67] which essentially correct the field with an hyperbolic method. There exists a large amount of literature on algorithms for solving this problem, coming as well from the mathematics as from the physics community, and a recent survey is available in [19]. However, despite some insightful studies on the proper discrete Gauss laws that should be preserved by a DG-PIC scheme [36, 48], we believe that the problem of designing a stable charge-conserving coupling for non-conforming solvers remained an open one. In this context the non-conforming methods obtained with our structure-preserving approach may be seen as general and satisfactory solution. Compared to existing DG-PIC schemes they offer an interesting alternative, since they naturally preserve a proper discrete version of the Gauss law and do not require divergence cleaning techniques for long-time stability.

The second contribution of this work is to specify such compatible and structure-preserving discretizations for the 2D Maxwell system

$$\begin{cases} \partial_t B + \operatorname{curl} \boldsymbol{E} = 0 \\ \partial_t \boldsymbol{E} - c^2 \, \mathbf{curl}\, B = -\dfrac{1}{\varepsilon_0} \boldsymbol{J} \end{cases} \tag{1.2}$$

of either conforming or non-conforming type. Here the two curl operators resulting from the dimensional reduction take the form $\operatorname{curl} \boldsymbol{u} = \partial_x u_y - \partial_y u_x$ for the scalar-valued operator and $\mathbf{curl}\, u = (\partial_y u, -\partial_x u)^T$ for the vector-valued one (using bold fonts to distinguish vector-valued entities).

By choice, the two methods proposed in this article include a discrete Ampère law in strong form. A dual option is done in our companion article [21], where two compatible schemes are proposed that include discrete Faraday laws in strong form. Here the first scheme is a standard conforming mixed finite element method involving discrete spaces of $H(\mathbf{curl})$ (i.e., H^1) and $\boldsymbol{H}(\mathrm{div})$ fields, for which we show that a Raviart-Thomas interpolation provides a Gauss-compatible approximation for the current $\boldsymbol{J}$. Our second scheme extends this construction to spaces of fully discontinuous fields as in standard DG

methods, in order to avoid inverting global mass matrices. It belongs to the class of Conforming/Non-conforming Galerkin (Conga) methods designed in [22] to preserve the mixed structure of conforming Galerkin approximations, and again we show that a compatible current approximation is provided by a Raviart-Thomas interpolation.

We then complete these two schemes by identifying for each of them the discrete divergence operators that form a complete structure-preserving discretizations in the sense defined above. In the case where the Maxwell system (1.2) is coupled with an additional equation for the source, such as a Vlasov equation, this framework allows us to show that the Raviart-Thomas finite element interpolation operators previously identified as Gauss-compatible for the Maxwell system alone can also be used to deposit the associated current $\boldsymbol{J} := q \int \boldsymbol{v} f \, \mathrm{d}\boldsymbol{v}$ (or better, its approximation by a moderate number of numerical particles) on the finite element spaces in a charge-conserving way, be it for the conforming or the non-conforming Galerkin discretization.

Finally, we provide numerical experiments that validate the approach and the numerical convergence of the proposed schemes (established by theoretical means for the Maxwell system alone), using a pure Maxwell problem and an academic Maxwell-Vlasov test case.

The outline is as follows: In Section 2 we present the theoretical framework and identify the discrete structure that enables us to obtain long time stability for the numerical solution of the Maxwell equations with exact or approximate sources. Then in Section 3 we introduce the Finite Element discretization and the appropriate conforming discretization framework for the Maxwell equations with a strong Ampère law. In Section 4 this is extended to fully discontinuous non-conforming elements where our framework enables us to construct compatible discretizations that are long time stable. To handle the case where the sources are themselves computed numerically from an auxiliary equation such as Vlasov, we then show in Section 5 that these Maxwell discretizations are structure-preserving when equipped with a proper discrete divergence, which allows us to derive charge-conserving deposition methods for the current. All these methods are finally validated and compared in Section 6 using a couple of relevant test problems.

2. Theoretical framework

In this section we describe the theoretical tools that will guide us throughout the construction of compatible and structure preserving Maxwell-PIC schemes with long-time stability properties. Overall, the idea of such methods is to reproduce at the discrete level the relations that guarantee the preservation of the Gauss laws in the exact solutions.

2.1. Two approaches to long-time stability

Let us give a formal overview of our stability analysis. If we rewrite the time-dependent Maxwell equations as

$$\partial_t U - \mathcal{A} U = -F \tag{2.1}$$

with $\mathcal{A} = c\begin{pmatrix} 0 & -\operatorname{curl} \\ \operatorname{curl} & 0 \end{pmatrix}$, and consider a space discretization of (2.1) under the form

$$\partial_t U_h - \mathcal{A}_h U_h = -F_h, \tag{2.2}$$

the main stability problem that we address here can be stated as: *Find a practical criterion to guarantee that when the exact source F gives rise to a solution U that is bounded in time, the approximate solution U_h is also bounded in time.*

Here by practical we mean a criterion that can be used in the design of a numerical scheme, and to have a more tractable problem we will first aim for stability with respect to *constant* sources. We also restrict ourselves to smooth solutions. Our approach then essentially consists in designing

proper approximation schemes for the source F, once a discrete curl operator $\mathcal{A}_h$ has been chosen with well-identified properties.

To answer this problem our first step is to use a Duhamel formula and write

$$U(t) = e^{t\mathcal{A}}U(0) + \int_0^t e^{(t-s)\mathcal{A}}F(s)\,\mathrm{d}s. \tag{2.3}$$

Here $\mathcal{A}$ is skew-symmetric and with close range, so that one has $(\ker\mathcal{A})^\perp = \operatorname{Im}\mathcal{A}$. We may then decompose a given source F as

$$F = F^{(0)} + \mathcal{A}G \ \in \ \ker\mathcal{A}\oplus(\ker\mathcal{A})^\perp = \ker\mathcal{A}\oplus\operatorname{Im}\mathcal{A} \tag{2.4}$$

and if we assume that F is constant, plugging this expression in (2.3) gives

$$U(t) - e^{t\mathcal{A}}U(0) = \int_0^t e^{(t-s)\mathcal{A}}F^{(0)}\,\mathrm{d}s - [e^{(t-s)\mathcal{A}}G]_0^t = tF^{(0)} + (e^{t\mathcal{A}} - I)G \tag{2.5}$$

which highlights the different roles played by sources in $\ker\mathcal{A}$ from those in its orthogogonal complement $\operatorname{Im}\mathcal{A}$: While the latter ones generate oscillating solutions that are bounded over time (due to the skew-symmetry of $\mathcal{A}$, $e^{t\mathcal{A}}$ is a contraction semi-group), the former ones give rise to solutions that grow linearly in time.

For the purpose of long-time accuracy we consider here discretizations that do not dissipate energy, leading to skew-symmetric operators $\mathcal{A}_h = -\mathcal{A}_h^*$. In particular a decomposition similar to (2.4) applies at the discrete level, as well as a discrete version of (2.5). It follows that a first solution is obtained by approximating F with an operator Π_h that satisfies the compatibility property

$$F \in \operatorname{Im}\mathcal{A} \qquad \Longrightarrow \qquad \Pi_h F \in \operatorname{Im}\mathcal{A}_h. \tag{2.6}$$

This approach has been followed in [22] where semi-discrete schemes of the form $\partial_t U_h - \mathcal{A}_h U_h = -\Pi_h F$ satisfying (2.6) have been studied and shown to have very good stability properties, especially with respect to steady-state solutions. In Section 2.3 we will recall the main properties of such schemes, and show that long-time stability estimates actually hold for almost every time harmonic solution.

In many cases of physical interest, however, the exact source F is not known. When solving the Maxwell-Vlasov system for example, the discrete current density F_h must be computed from an approximate density provided by some Vlasov solver, e.g. from numerical particles in the case of a PIC method. In such cases the property (2.6) is of little help as one cannot use F to compute F_h, and we must rely on another stability criterion.

For this purpose we propose an alternative stability analysis. Its starting point lies in the observation that, despite being called *Gauss-compatible* in [22], Maxwell discretizations of the form $\partial_t U_h - \mathcal{A}_h U_h = -\Pi_h F$ satisfying (2.6) do not make an explicit use of the Gauss laws which we may rewrite here as

$$\mathcal{D}U = R \tag{2.7}$$

with $\mathcal{D} = \left(\begin{smallmatrix}\mathrm{div} & 0\\ 0 & \mathrm{div}\end{smallmatrix}\right)$. To derive a more robust analysis we then rely on two key properties that are known to be important for stability purposes in general, namely: (i) a property of the kernels,

$$\ker\mathcal{D} = (\ker\mathcal{A})^\perp \tag{2.8}$$

that corresponds to an exact sequence property, and (ii) Poincaré estimates of the form

$$\begin{cases}\|Z\| \le c_P\|\mathcal{A}Z\|, & Z\in(\ker\mathcal{A})^\perp\\ \|Z\| \le c_P\|\mathcal{D}Z\|, & Z\in(\ker\mathcal{D})^\perp\end{cases} \tag{2.9}$$

(unless specified otherwise, $\|\cdot\|$ denotes L^2 norms throughout the article). Property (2.8) then allows us to decompose any solution of the full Maxwell system as $U = U^{\mathcal{D}\perp} + U^{\mathcal{A}\perp} \in (\ker\mathcal{A})^\perp \oplus (\ker\mathcal{D})^\perp$,

and, assuming again a constant source F, estimate

$$\|U(t)\| \leq \|U^{\mathcal{D}\perp}(t)\| + \|U^{\mathcal{A}\perp}(t)\| \leq c_P\big(\|\mathcal{D}U(t)\| + \|\mathcal{A}U(t)\|\big) \leq c_P\big(\|R(t)\| + \|\mathcal{A}U(0)\| + 2\|F\|\big) \quad (2.10)$$

where we have used a computation similar to (2.5) in the last bound. A second solution to our numerical stability problem is then obtained by reproducing these steps at the discrete level, as follows. Given a stable discretization $\mathcal{A}_h$ of the curl operators, i.e., a skew-symmetric operator $\mathcal{A}_h$ which satisfies a Poincaré estimate

$$\|Z\| \leq c_P\|\mathcal{A}_h Z\|, \quad Z \in (\ker \mathcal{A}_h)^\perp \quad (2.11)$$

uniformly in h, we propose to:

(i) find a discrete divergence operator $\mathcal{D}_h$ that is also stable

$$\|Z\| \leq c_P\|\mathcal{D}_h Z\|, \quad Z \in (\ker \mathcal{D}_h)^\perp \quad (2.12)$$

uniformly in h, and satisfies the discrete kernel property

$$\ker \mathcal{D}_h = (\ker \mathcal{A}_h)^\perp, \quad (2.13)$$

(ii) compute the discrete current F_h from the approximate solution provided by the coupled (e.g., Vlasov) solver in such a way that the discrete continuity equation

$$\partial_t R_h + \mathcal{D}_h F_h = 0 \quad (2.14)$$

holds with R_h a reasonnable approximation of the charge density computed by the coupled solver.

Indeed, it is easily verified that the steps above lead to the proper discrete Gauss law

$$\mathcal{D}_h U_h = R_h \quad (2.15)$$

to be preserved in time by the solutions to (2.2), and that a long-time stability estimate similar to (2.10) holds for U_h. This solves our stability problem since R_h will be bounded in time if the Vlasov solver is stable, even if no relation like (2.6) holds for F_h.

In Section 2.4 we will detail such a construction using more telling notations. Discretizations of the original equations in terms of discrete operators $\mathcal{A}_h$ and $\mathcal{D}_h$ satisfying properties (2.11), (2.13) and (2.12) above will be said *structure-preserving*. If in addition the approximate source is computed in such a way that the proper continuity equation (2.14) is satisfied, then the schemes will be called *charge-conserving* to follow the common terminology.

2.2. **Time-dependent 2D Maxwell system in operator form**

We now specify an operator form for the Maxwell system (1.2) that will allow us to perform the stability analysis outlined above, and serve as a reference for the subsequent conforming and non-conforming Galerkin schemes.

Throughout the article we assume that the domain Ω is bounded, simply connected and Lipschitz. Moreover, to keep the presentation as simple as possible we restrict ourselves to the case of metallic boundary conditions

$$\boldsymbol{E} \times \boldsymbol{n} = 0 \qquad \text{on} \quad \partial\Omega \quad (2.16)$$

and leave the case of absorbing boundary conditions for a future study. We note that in 2D the cross product with a vector $\boldsymbol{u}$ maps vectors to scalars and vice-versa,

$$\boldsymbol{u} \times \boldsymbol{v} = u_x v_y - u_y v_x \qquad \text{and} \qquad \boldsymbol{u} \times v = \begin{pmatrix} u_y v \\ -u_x v \end{pmatrix}.$$

To highlight the functional structure of the subsequent constructions we borrow some notations from Finite Element Exterior Calculus (FEEC), see e.g., [2, 3, 4]. We denote

$$W^0 := \mathbb{R}, \qquad W^1 := L^2(\Omega), \qquad W^2 := L^2(\Omega)^2, \qquad W^3 := L^2(\Omega) \tag{2.17}$$

with standard notations for Hilbert spaces, see e.g. [35]. We next consider closed and densely-defined operators d^l from W^l to W^{l+1}, namely

$$d^0 := \iota, \qquad d^1 := \mathbf{curl} \qquad \text{and} \qquad d^2 := \mathrm{div}$$

where ι denotes the canonical injection from $\mathbb{R}$ to $L^2(\Omega)$, with respective domains

$$V^0 := D(d^0) = \mathbb{R}, \qquad V^1 := D(d^1) = H(\mathbf{curl}, \Omega) \qquad \text{and} \qquad V^2 := D(d^2) = \boldsymbol{H}(\mathrm{div}, \Omega). \tag{2.18}$$

A word on the notation: our main motivation here for bold-face to denote vector-valued fields, operators and spaces is to make a clear distinction between the two curl operators (one being the dual of the other). Because the confusion cannot be made on the d^l operators, we shall not use bold-face on the d^l or V^l notation although some of them correspond to vector-valued fields. This also allows us to state general definitions and results that readily extend to the 3D case, see Definition 2.12 and Remark 2.21 below.

Setting then $V^3 := W^3 = L^2(\Omega)$ and using standard results we next observe that if Ω is a bounded and simply-connected Lipschitz domain, then the following sequence is exact

$$V^0 \xrightarrow{d^0=\iota} V^1 \xrightarrow{d^1=\mathbf{curl}} V^2 \xrightarrow{d^2=\mathrm{div}} V^3 \xrightarrow{0} \{0\} \tag{2.19}$$

in the sense that the range of each operator coincides with the kernel of the following operator, see e.g. [75, Cor. 3.16]. We then denote by $(d^2)^*$, $(d^1)^*$ and $(d^0)^*$ the adjoints of d^2, d^1 and d^0 respectively: their domains are

$$V_3^* := D((d^2)^*) = H_0^1(\Omega), \qquad V_2^* := D((d^1)^*) = \boldsymbol{H}_0(\mathrm{curl}, \Omega) \qquad V_1^* := D((d^0)^*) = L^2(\Omega)$$

and on these domains they coincide with the operators $-\mathbf{grad}$, curl and $\fint_\Omega : u \mapsto |\Omega|^{-1} \int_\Omega u$, respectively. (Here the space numbering follows the standard convention [4, Sec. 3.1] and is motivated by the fact that V_{l+1}^* is then a subspace of W^{l+1}.) Setting $V_0^* := W^0 = \mathbb{R}$ and using duality arguments based on the fact that all the operators are densely-defined and with a closed range in L^2, we then find that the following sequence is also exact,

$$\{0\} \xrightarrow{0} V_3^* \xrightarrow{(d^2)^*=-\mathbf{grad}} V_2^* \xrightarrow{(d^1)^*=\mathrm{curl}} V_1^* \xrightarrow{(d^0)^*=\fint_\Omega} V_0^* \tag{2.20}$$

Remark 2.1. Note that the V_l^*'s are not dual to the V^l's. Indeed, the dual spaces involved in the definition of the adjoint operators $(d^l)^*$ are those of the W^l's, which (as L^2 spaces) are identified with themselves.

In this setting we define $\mathcal{A}$ as the unbounded operator from $\mathcal{W} := W^1 \times W^2$ to itself defined by

$$\mathcal{A} := c \begin{pmatrix} 0 & -(d^1)^* \\ d^1 & 0 \end{pmatrix} = c \begin{pmatrix} 0 & -\mathrm{curl} \\ \mathbf{curl} & 0 \end{pmatrix} \tag{2.21}$$

with domain

$$\mathcal{V} := D(\mathcal{A}) = V^1 \times V_2^* = H(\mathbf{curl}, \Omega) \times \boldsymbol{H}_0(\mathrm{curl}, \Omega).$$

This "composite" operator is classical, see e.g., [1, 23, 76], and as seen above it allows to represent in a unified way the action of the two curls involved in the Maxwell equations. Writing $U = (cB, \mathbf{E})^T$ and $F = (0, \varepsilon_0^{-1}\boldsymbol{J})^T$ we can indeed reformulate the time-dependent Maxwell system (1.2) with metallic boundary conditions (2.16) as

$$\partial_t U - \mathcal{A}U = -F. \tag{2.22}$$

Standard arguments guarantee the well-posedness of the above equation complemented with an initial condition and a smooth source term. Indeed, it can be verified that $\mathcal{A}$ is skew-symmetric in the sense that $\mathcal{A}^* = -\mathcal{A}$. In particular it generates a contraction semi-group of class $\mathcal{C}_0$ (see [74, Section IX.8]) and the following result is a direct application of Corollaries 2.2 (p. 106) and 2.5 (p. 107) in [62].

Lemma 2.2. *If $F \in \mathcal{C}^1([0,T];\mathcal{W})$, then the Cauchy problem (2.22) complemented with an arbitrary initial condition $U^0 \in \mathcal{V}$ has a unique solution $U \in \mathcal{C}^0([0,T[;\mathcal{V})$ that is continuously differentiable on $]0,T[$.*

Turning to the Gauss laws, we observe that even if the divergence of a magnetic field of the form $\boldsymbol{B} = (0,0,B)$ is always zero, there actually *is* a non-trivial constraint analogous to the electric Gauss law

$$\operatorname{div} \boldsymbol{E} = \frac{1}{\varepsilon_0}\rho \tag{2.23}$$

that should be imposed on the magnetic field B in the 2D setting. It is obtained by considering that, just as the relation $\operatorname{div}\mathbf{curl}\, B = 0$ guarantees the preservation of the electric Gauss law, the relation $\int_\Omega \operatorname{curl} \boldsymbol{E} = \int_{\partial\Omega} \boldsymbol{n} \times \boldsymbol{E} = 0$, derived from the metallic boundary conditions, guarantees that

$$\int_\Omega B = \int_\Omega B^0 \tag{2.24}$$

where $B^0 = B(t=0)$, holds for all $t \geq 0$. We may then see this equation as the relevant magnetic Gauss law in the reduced 2D model, an interpretation that will be supported by the stability analysis developed in this work.

The Gauss laws (2.23) and (2.24) can then be recast in the compact form

$$\mathcal{D}U = R \tag{2.25}$$

where the "composite" divergence $\mathcal{D}$ is the unbounded operator defined from $\mathcal{W} = W^1 \times W^2$ to $W^0 \times W^3$ by

$$\mathcal{D} := \begin{pmatrix} (d^0)^* & 0 \\ 0 & d^2 \end{pmatrix} = \begin{pmatrix} \int_\Omega & 0 \\ 0 & \operatorname{div} \end{pmatrix} \tag{2.26}$$

with domain

$$D(\mathcal{D}) = V_1^* \times V^2 = L^2(\Omega) \times \boldsymbol{H}(\operatorname{div},\Omega)$$

and where $R := (\int_\Omega cB^0, \varepsilon_0^{-1}\rho)^T$ represents the composite charge density in this 2D model, consistent with our interpretation of (2.24) as a generalized Gauss law for the scalar magnetic field. Using the exact sequence (2.19) and a standard property of adjoint operators, see e.g., [12, Cor. 2.18], we see that $\ker d^2 = d^1 V^1 = \operatorname{Im} d^1 = (\ker(d^1)^*)^\perp$ (here and below, the $\perp$ exponent denotes the orthogonal complement in the natural Hilbert space) and it follows that

$$\ker \mathcal{D} = \mathbb{R}^\perp \times \ker d^2 = (\ker d^1)^\perp \times (\ker(d^1)^*)^\perp = (\ker \mathcal{A})^\perp. \tag{2.27}$$

Thus, in the absence of sources the Gauss law (2.25) can be seen as a constraint that forces the solutions of the Ampère-Faraday system (2.22) to be orthogonal to the curl-free fields, which correspond to the *genuinely oscillating* modes of the linear operator $\mathcal{A}$. Indeed, using again the skew-symmetry of $\mathcal{A}$ we can decompose the L^2 space $\mathcal{W} = W^1 \times W^2$ as

$$\mathcal{W} = \ker \mathcal{A} \,\oplus\, (\ker \mathcal{A})^\perp \qquad \text{with} \qquad \begin{cases} \ker \mathcal{A} = \{U \in \mathcal{S} : \partial_t U = 0\} \\ (\ker \mathcal{A})^\perp = \operatorname{Span}(\{U \in \mathcal{S} : \partial_t U = i\omega U\} : \omega \neq 0) \end{cases} \tag{2.28}$$

where $\mathcal{S}$ denotes the solutions to the homogeneous Ampère-Faraday system (2.22).

2.3. **Gauss-compatible solvers for the Maxwell equations with exact sources**

In the case where the exact source F is known we may consider semi-discrete schemes for (2.22) of the form

$$\partial_t U_h - \mathcal{A}_h U_h = -\Pi_h F \tag{2.29}$$

where $\mathcal{A}_h : \mathcal{V}_h \to \mathcal{V}_h$ is a skew-symmetric operator approximating $\mathcal{A}$ on a finite-dimensional space $\mathcal{V}_h \subset \mathcal{W}$, and Π_h is an approximation operator mapping on $\mathcal{V}_h$.

As recalled above, a simple criterion has been proposed in [22] to characterize schemes of the above form that are stable for constant sources. In the source-free case this criterion (2.6) amounts to preserving the relation $U_h \in (\ker \mathcal{A}_h)^\perp$ which can be seen as a discrete analog of the orthogonal constraint expressed by the Gauss laws ($U \in \ker \mathcal{D} = (\ker \mathcal{A})^\perp$), and for this reason the associated schemes have been called *Gauss-compatible*. Since $(\ker \mathcal{A})^\perp$ and $(\ker \mathcal{A}_h)^\perp$ respectivelly coincide with $\operatorname{Im} \mathcal{A}$ and $\operatorname{Im} \mathcal{A}_h$, the compatibility condition (2.6) is essentially expressed with a commuting diagram. For the purpose of the current article we introduce the following definition in the spirit of [22].

Definition 2.3. We say that a discrete operator $\mathcal{A}_h : \mathcal{V}_h \to \mathcal{V}_h$ forms a **Gauss-compatible approximation** of $\mathcal{A}$ together with a mapping Π_h on $\mathcal{V}_h$ if there exists an auxiliary mapping $\hat{\Pi}_h : \hat{\mathcal{V}} \to \mathcal{V}_h$ that converges pointwise to the identity as $h \to 0$, and that is such that

$$\Pi_h \mathcal{A} = \mathcal{A}_h \hat{\Pi}_h \tag{2.30}$$

holds on $\hat{\mathcal{V}}$.

Remark 2.4. The purpose of the pointwise convergence property in the above definition is to avoid trivial operators. It will not be used in the subsequent error and stability estimates.

We observe that (2.30) indeed amounts to writing that the following diagram commutes:

$$\begin{array}{ccc} \hat{\mathcal{V}} & \xrightarrow{\ \mathcal{A}\ } & \mathcal{A}\hat{\mathcal{V}} \\ \Big\downarrow{\scriptstyle \hat{\Pi}_h} & & \Big\downarrow{\scriptstyle \Pi_h} \\ \mathcal{V}_h & \xrightarrow{\ \mathcal{A}_h\ } & \mathcal{V}_h \end{array} \tag{2.31}$$

and this commuting diagram yields an a priori error estimate leading to long-time stability properties, as shown by the following results which slightly extend the a priori estimates from [22, Sec. 3].

Theorem 2.5. *If the semi-discrete scheme* (2.29) *is Gauss-compatible in the sense of Definition 2.3, then the approximate solution satisfies*

$$\|(U_h - \hat{\Pi}_h U)(t)\| \le \|(U_h - \hat{\Pi}_h U)(0)\| + \Big\| \int_0^t e^{(t-s)\mathcal{A}_h} (\hat{\Pi}_h - \Pi_h) \partial_t U(s)\, \mathrm{d}s \Big\| \tag{2.32}$$

for any solution $U \in \mathcal{C}^0([0,T]; \hat{\mathcal{V}})$ to the time-dependent Maxwell system (2.22).

Proof. Applying the projection Π_h to the Maxwell system (2.22) and using the commuting diagram property yields

$$\partial_t \Pi_h U - \mathcal{A}_h \hat{\Pi}_h U = \Pi_h(\partial_t U - \mathcal{A} U) = -\Pi_h F = \partial_t U_h - \mathcal{A}_h U_h,$$

from which we see that $\hat{\Pi}_h U - U_h$ satisfies an evolution equation with source term $(\hat{\Pi}_h - \Pi_h)\partial_t U$,

$$\partial_t(\hat{\Pi}_h U - U_h) - \mathcal{A}_h(\hat{\Pi}_h U - U_h) = (\hat{\Pi}_h - \Pi_h)\partial_t U.$$

Estimate (2.32) then follows by applying a discrete Duhamel formula and using the contraction properties of the semi-group generated by $\mathcal{A}_h$. ∎

In Remark 2.10 below we summarize the main benefits of our error analysis, but before we derive a couple of useful corollaries from the skew-symmetry of $\mathcal{A}_h$.

Corollary 2.6 (standard error estimate)**.** *Using the contraction properties of the semi-group $e^{t\mathcal{A}_h}$, one infers from* (2.32) *that*

$$\|(U_h - \hat{\Pi}_h U)(t)\| \leq \|(U_h - \hat{\Pi}_h U)(0)\| + \int_0^t \|(\hat{\Pi}_h - \Pi_h)\partial_t U(s)\| \, \mathrm{d}s. \tag{2.33}$$

In Sections 3.4 and 4.2 we will use (2.33) to establish convergence estimates for the proposed conforming and non-conforming schemes. In [22] we have emphasized that (2.33) implies a long-time stability property with respect to steady-state solutions, and here we use (2.32) to further observe that the Gauss-compatibility actually provide long-time stability with respect to almost every time-harmonic solution.

Corollary 2.7 (long-time stability for time harmonic solutions)**.** *Let* (2.29) *be a Gauss-compatible scheme in the sense of Definition 2.3, and let $U(t,x) = e^{i\omega t}U(0,x)$ be a time-harmonic solution to* (2.22) *with $U(0,\cdot) \in \hat{\mathcal{V}}$ and $i\omega \notin \sigma_*(\mathcal{A}_h)$ where $\sigma_*(\mathcal{A}_h) := \sigma(\mathcal{A}_h) \setminus \{0\}$. Then the semi-discrete solution satisfies*

$$\|(U_h - \hat{\Pi}_h U)(t)\| \leq \|(U_h - \hat{\Pi}_h U)(0)\| + \Big(1 + \Big|\frac{\omega}{\operatorname{dist}(i\omega, \sigma_*(\mathcal{A}_h))}\Big|\Big)\|2(\hat{\Pi}_h - \Pi_h)U(0)\| \tag{2.34}$$

for all $t \geq 0$.

Proof. In the case where $\omega = 0$, the result readily follows from (2.33). Otherwise we have $i\omega \notin \sigma(\mathcal{A}_h)$. Using the skew-symmetry of $\mathcal{A}_h$ we then equip $\mathcal{V}_h$ with an orthonormal basis of eigenvectors $Z_{h,j}$, $j = 1, \ldots, N_h$, associated with imaginary eigenvalues $i\omega_{h,j} \in i\mathbb{R}$. We then decompose

$$(\hat{\Pi}_h - \Pi_h)U(t,x) = e^{i\omega t}(\hat{\Pi}_h - \Pi_h)U(0,x) = e^{i\omega t}\sum_j \delta_{h,j} Z_{h,j}(x) \tag{2.35}$$

and we compute that

$$\int_0^t e^{(t-s)\mathcal{A}_h}(\hat{\Pi}_h - \Pi_h)\partial_t U(s)\,\mathrm{d}s = i\omega \sum_j e^{i\omega_{h,j}t}\delta_{h,j}\int_0^t e^{i(\omega-\omega_{h,j})s}Z_{h,j}\,\mathrm{d}s = \omega\sum_j \frac{e^{i\omega t} - e^{i\omega_{h,j}t}}{\omega - \omega_{h,j}}\delta_{h,j}Z_{h,j}.$$

Observing that $\big|\frac{\omega}{\omega-\omega_{h,j}}\big| \leq 1 + \big|\frac{\omega}{\operatorname{dist}(i\omega,\sigma_*(\mathcal{A}_h))}\big|$ for all j, we then find

$$\Big\|\int_0^t e^{(t-s)\mathcal{A}_h}(\hat{\Pi}_h - \Pi_h)\partial_t U(s)\,\mathrm{d}s\Big\|^2 \leq \Big(1 + \Big|\frac{\omega}{\operatorname{dist}(i\omega,\sigma_*(\mathcal{A}_h))}\Big|\Big)^2 \sum_j |2\delta_{h,j}|^2$$

and Estimate (2.34) follows by noting that $\sum_j |2\delta_{h,j}|^2 = \|2(\hat{\Pi}_h - \Pi_h)U(0)\|^2$ holds thanks to the orthonormal decomposition (2.35). ∎

Remark 2.8. As noted above, our stability results cover the case of steady state solutions ($\omega = 0$) and in fact an important asset of (2.34) is that it is not affected by the large kernel of $\mathcal{A}_h$. In addition, we observe that if the eigenvalues of $\mathcal{A}_h$ converge towards those of $\mathcal{A}$ in the sense that for all $\eta > 0$ there exists h_0 such that $\operatorname{dist}(i\omega_{h,j}, \sigma_*(\mathcal{A})) \leq \eta$ holds for all $h \leq h_0$ and $i\omega_{h,j} \in \sigma_*(\mathcal{A}_h)$, where

$$\sigma_*(\mathcal{A}) := \sigma(\mathcal{A}) \setminus \{0\}$$

denotes the discrete spectrum of $\mathcal{A}$, then by taking $\eta = \frac{1}{2}\operatorname{dist}(i\omega, \sigma_*(\mathcal{A}))$ we find that

$$\|(U_h - \hat{\Pi}_h U)(t)\| \leq \|(U_h - \hat{\Pi}_h U)(0)\| + \Big(1 + \Big|\frac{2\omega}{\operatorname{dist}(i\omega, \sigma_*(\mathcal{A}))}\Big|\Big)\|2(\hat{\Pi}_h - \Pi_h)U(0)\|$$

holds for all $h \leq h_0$ and $t \geq 0$. (Despite being close, we note however that this convergence property is not guaranteed by the classical Definition 2.1 proposed in [7] for the spectral correctness.)

Remark 2.9. In the case of time-harmonic solutions U oscillating with a frequency $i\omega$ in the discrete spectrum $\sigma_*(\mathcal{A})$, we see that F cannot have a component along the eigenspace $\ker(i\omega I - \mathcal{A})$, but it would be too strong to ask that a similar property holds also for its approximation F_h. Although this prevents us from establishing long-time stability estimates for arbitrary frequencies, in practice such kind of instabilities are not likely to be important, indeed they can only be triggered by a (residual) contribution in $\ker(i\omega_{h,j} I - \mathcal{A}_h)$ that oscillates at the exact frequency $\omega_{h,j}$.

Remark 2.10 (benefits of this error analysis)**.** Overall, the above results (combined with approximation error estimates for the operators Π_h and $\hat{\Pi}_h$) gives a general tool to derive error estimates with long-time stability properties when the source approximation scheme satisfies the compatibility criterion (2.30). In the cases where the natural L^2 projection is a compatible approximation operator, we note that classical estimates leading to long-time stability are known already, see e.g. Th. 2.1 in [54] under commuting assumptions that are similar to the ones involved in our compatibility Definition 2.3, or Th. 3.1 in [50] and Th. 4.1 in [76]. The benefit of our analysis is twofold: first, it allows to extend stable estimates to conforming Maxwell solvers where the L^2 projections may not lead to stable schemes, see Section 6.1, and to easily identify a compatible approximation operator for the source. Second it naturally applies to non-conforming discretizations, as will be verified with the Conga schemes studied in Section 4.2 below and in our companion article [21], following the method proposed in [22] for the 3D Maxwell system.

As pointed in the introduction, a third benefit of our approach is to allow to derive stable estimates in the case of approximate sources. This relies on the notion of structure-preserving and charge-conserving schemes, and is the subject of the next section.

2.4. The case of approximate sources: stability through structure preservation

In the cases where the exact current density is not known the analysis of [22] does not apply, as explained in Section 2.1 above. Indeed one needs to consider schemes of the form

$$\partial_t U_h - \mathcal{A}_h U_h = -F_h \tag{2.36}$$

where F_h is a given approximation of the exact current source $F = (0, \varepsilon_0^{-1}\boldsymbol{J})^T$ that may not be compatible in the sense of (2.6).

For such problems we rely on the second stability approach outlined in Section 2.1, which consists of building discretizations that satisfy (2.11), (2.12) and (2.13). Using duality arguments (see Lemma 2.15 below), these properties can be expressed on the discretization of one sequence only, either the primal (2.19) or the dual one (2.20). We start with the primal one.

Definition 2.11. We say that a semi-discrete 2D Maxwell system of the form

$$\begin{cases} \partial_t B_h + \mathrm{curl}_h\, \boldsymbol{E}_h = 0 \\ \partial_t \boldsymbol{E}_h - c^2\, \mathbf{curl}_h\, B_h = -\dfrac{1}{\varepsilon_0}\boldsymbol{J}_h \end{cases} \quad \text{with} \quad \begin{cases} \mathbf{curl}_h : V_h^1 \to V_h^2 \\ \mathrm{curl}_h := (\mathbf{curl}_h)^* : V_h^2 \to V_h^1 \end{cases} \tag{2.37}$$

completed with discrete Gauss laws of the form

$$\begin{cases} \mathrm{div}_h\, \boldsymbol{E}_h = \dfrac{1}{\varepsilon_0}\rho_h \\ (\iota_h)^* B_h = (\iota_h)^* B_h^0 \end{cases} \quad \text{with} \quad \begin{cases} \mathrm{div}_h : V_h^2 \to V_h^3 \\ \iota_h : V_h^0 \to V_h^1 \end{cases} \tag{2.38}$$

is **structure-preserving** if the following properties hold.

- *Exact sequence property*: the sequence

$$V_h^0 \xrightarrow{\ \iota_h\ } V_h^1 \xrightarrow{\ \mathbf{curl}_h\ } V_h^2 \xrightarrow{\ \mathrm{div}_h\ } V_h^3 \tag{2.39}$$

is exact, in the sense that $\iota_h V_h^0 = \ker \mathbf{curl}_h$ and $\mathbf{curl}_h V_h^1 = \ker \mathrm{div}_h$.

- *Stability*: the operators in the above sequence satisfy Poincaré estimates,

$$\begin{aligned} &\|u\| \le c_P \|\iota_h u\|, && u \in V_h^0 \cap (\ker \iota_h)^\perp \\ &\|u\| \le c_P \|\mathbf{curl}_h\, u\|, && u \in V_h^1 \cap (\ker \mathbf{curl}_h)^\perp \\ &\|\boldsymbol{u}\| \le c_P \|\mathrm{div}_h\, \boldsymbol{u}\|, && \boldsymbol{u} \in V_h^2 \cap (\ker \mathrm{div}_h)^\perp \end{aligned} \tag{2.40}$$

with a constant c_P independent of h.

Here the presence of a discrete injection operator ι_h is due to the 2D setting: for the 3D problem it should be replaced by a discrete gradient operator. In fact our stability analysis readily applies to other formulations such as the strong Faraday form of Maxwell's equations studied in our companion paper [21] or to the 3D model. To highlight its generality we reformulate Definition 2.11 in terms of operators d_h^l approximating the d^l's on discrete spaces $V_h^l \subset W^l$, see (2.17)-(2.18).

Definition 2.12. We say that a semi-discrete 2D Maxwell system of the form

$$\begin{cases} \partial_t B_h + (d_h^1)^* \boldsymbol{E}_h = 0 \\ \partial_t \boldsymbol{E}_h - c^2 d_h^1 B_h = -\dfrac{1}{\varepsilon_0} \boldsymbol{J}_h \end{cases} \quad \text{with} \quad \begin{cases} d_h^1 : V_h^1 \to V_h^2 \\ (d_h^1)^* : V_h^2 \to V_h^1 \end{cases} \tag{2.41}$$

completed with discrete Gauss laws of the form

$$\begin{cases} d_h^2 \boldsymbol{E}_h = \dfrac{1}{\varepsilon_0} \rho_h \\ (d_h^0)^* B_h = (d_h^0)^* B_h^0 \end{cases} \quad \text{with} \quad \begin{cases} d_h^2 : V_h^2 \to V_h^3 \\ d_h^0 : V_h^0 \to V_h^1 \end{cases} \tag{2.42}$$

is **structure-preserving** if the following properties hold.

- *Exact sequence property*: the sequence

$$V_h^0 \xrightarrow{\ d_h^0\ } V_h^1 \xrightarrow{\ d_h^1\ } V_h^2 \xrightarrow{\ d_h^2\ } V_h^2 \tag{2.43}$$

is exact, in the sense that $d_h^0 V_h^0 = \ker d_h^1$ and $d_h^1 V_h^1 = \ker d_h^2$.

- *Stability*: the operators in the above sequence satisfy Poincaré estimates

$$\begin{aligned} &\|u\| \le c_P \|d_h^0 u\|, && u \in V_h^0 \cap (\ker d_h^0)^\perp \\ &\|u\| \le c_P \|d_h^1 u\|, && u \in V_h^1 \cap (\ker d_h^1)^\perp \\ &\|\boldsymbol{u}\| \le c_P \|d_h^2 \boldsymbol{u}\|, && \boldsymbol{u} \in V_h^2 \cap (\ker d_h^2)^\perp \end{aligned} \tag{2.44}$$

with a constant c_P independent of h.

These properties can be equivalently stated on the discretization of the dual sequence (2.20).

Lemma 2.13. *The exactness of the sequence* (2.43) *is equivalent to the one of*

$$V_h^3 \xrightarrow{\ (d_h^2)^*\ } V_h^2 \xrightarrow{\ (d_h^1)^*\ } V_h^1 \xrightarrow{\ (d_h^0)^*\ } V_h^0 \tag{2.45}$$

and the stability estimates (2.44) *hold if and only if the adoint operators satisfy*

$$\begin{aligned} &\|u\| \le c_P \|(d_h^2)^* u\|, && u \in V_h^3 \cap (\ker (d_h^2)^*)^\perp \\ &\|\boldsymbol{u}\| \le c_P \|(d_h^1)^* \boldsymbol{u}\|, && \boldsymbol{u} \in V_h^2 \cap (\ker (d_h^1)^*)^\perp \\ &\|u\| \le c_P \|(d_h^0)^* u\|, && u \in V_h^1 \cap (\ker (d_h^0)^*)^\perp. \end{aligned} \tag{2.46}$$

Proof. The arguments are standard. The implication $d_h^{l-1}V_h^{l-1} = \ker d_h^l \implies (d_h^l)^* V_h^{l+1} = \ker(d_h^{l-1})^*$ follows from the relations

$$(d_h^l)^* V_h^{l+1} = V_h^l \cap (\ker d_h^l)^\perp \qquad \text{and} \qquad \ker(d_h^{l-1})^* = V_h^l \cap (d_h^{l-1}V_h^{l-1})^\perp \tag{2.47}$$

which are easily inferred from the basic properties of the discrete adjoints, and the reverse implication follows by symmetry. Next take $u \in V_h^{l+1} \cap (\ker(d_h^l)^*)^\perp$: using (2.47) we see that $u \in d_h^l V_h^l$, so that there exists $v \in V_h^l \cap (\ker d_h^l)^\perp$ such that $d_h^l v = u$. In particular, if d_h^l is stable in the sense of (2.44) we have $\|v\| \leq c_P \|u\|$, which allows to write

$$\|u\| \leq c_P \frac{\|u\|^2}{\|v\|} = c_P \frac{\langle u, d_h^l v\rangle}{\|v\|} = c_P \frac{\langle (d_h^l)^* u, v\rangle}{\|v\|} \leq c_P \|(d_h^l)^* u\|.$$

This shows that $(d_h^l)^*$ is stable in the sense of (2.46), and the proof is completed by symmetry. ∎

In the terms of Definition 2.11, this gives the following result.

Lemma 2.14. *The space-discretization* (2.37)-(2.38) *is structure-preserving if and only if the following properties hold:*

- *letting* $\mathbf{grad}_h := -(\mathrm{div}_h)^*$*, the dual discrete sequence*

$$V_h^3 \xrightarrow{\mathbf{grad}_h} V_h^2 \xrightarrow{\mathrm{curl}_h} V_h^1 \xrightarrow{(\iota_h)^*} V_h^0 \tag{2.48}$$

  is exact, in the sense that $\mathbf{grad}_h V_h^3 = \ker \mathrm{curl}_h$ *and* $\mathrm{curl}_h V_h^2 = \ker(\iota_h)^*$*,*

- *the operators in the above sequence satisfy*

$$\begin{aligned} &\|u\| \leq c_P \|\mathbf{grad}_h u\|, && u \in V_h^3 \cap (\ker \mathbf{grad})^\perp \\ &\|\boldsymbol{u}\| \leq c_P \|\mathrm{curl}_h \boldsymbol{u}\|, && \boldsymbol{u} \in V_h^2 \cap (\ker \mathrm{curl}_h)^\perp \\ &\|u\| \leq c_P \|(\iota_h)^* u\|, && u \in V_h^1 \cap (\ker(\iota_h)^*)^\perp. \end{aligned} \tag{2.49}$$

  with a constant c_P *independent of* h*.*

Finally, we verify that the above definition indeed corresponds to the key stability properties announced in Section 2.1.

Lemma 2.15. *The properties* (2.39)-(2.40)*, or equivalently* (2.48)-(2.49)*, hold if and only if the composite curl and divergence operators*

$$\mathcal{A}_h := c \begin{pmatrix} 0 & -\mathrm{curl}_h \\ \mathbf{curl}_h & 0 \end{pmatrix} : (V_h^1 \times V_h^2) \to (V_h^1 \times V_h^2), \qquad \mathcal{D}_h := \begin{pmatrix} (\iota_h)^* & 0 \\ 0 & \mathrm{div}_h \end{pmatrix} : (V_h^1 \times V_h^2) \to (V_h^0 \times V_h^3)$$

or

$$\mathcal{A}_h := c \begin{pmatrix} 0 & -(d_h^1)^* \\ d_h^1 & 0 \end{pmatrix} : (V_h^1 \times V_h^2) \to (V_h^1 \times V_h^2), \qquad \mathcal{D}_h := \begin{pmatrix} (d_h^0)^* & 0 \\ 0 & d_h^2 \end{pmatrix} : (V_h^1 \times V_h^2) \to (V_h^0 \times V_h^3)$$

in the notation of Definition 2.12, satisfy (2.11)*,* (2.12) *and* (2.13)*.*

Proof. Since $\mathcal{A}_h$ is skew-symmetric by construction, we have $(\ker \mathcal{A}_h)^\perp = \mathrm{Im}\, \mathcal{A}_h$ and the kernel compatibility (2.13) is equivalent to a couple of exact sequence properties, namely

$$\ker \mathrm{div}_h = \mathbf{curl}_h V_h^1 \qquad \text{and} \qquad \ker(\iota_h)^* = \mathrm{curl}_h V_h^2. \tag{2.50}$$

By duality (see Lemma 2.14) the latter is equivalent to $\mathrm{Im}\, \iota_h = \ker \mathbf{curl}_h$, so that (2.50) is indeed equivalent to the exact sequence property (2.39). As for the uniform stability properties (2.11)-(2.12), they can be restated as four estimates: the second and third ones in (2.40) and two more, namely

$$\|\boldsymbol{u}\| \leq c_P \|\mathrm{curl}_h \boldsymbol{u}\|, \quad \boldsymbol{u} \in (\ker \mathrm{curl}_h)^\perp \qquad \text{and} \qquad \|u\| \leq c_P \|(\iota_h)^* u\|, \quad u \in (\ker(\iota_h)^*)^\perp \tag{2.51}$$

which are equivalent to their primal counterparts as seen also in Lemma 2.14. ∎

Definition 2.16. We say that a semi-discrete Maxwell system of the form

$$\begin{cases} \partial_t U_h - \mathcal{A}_h U_h = -F_h \\ \qquad\quad \mathcal{D}_h U_h = R_h \end{cases} \tag{2.52}$$

with $\mathcal{A}_h$ a skew-symmetric operator, is **charge-conserving** if

(i) it is structure-preserving in the sense that properties (2.11), (2.12) and (2.13) hold,

(ii) and the approximate sources satisfy the corresponding discrete continuity equation

$$\partial_t R_h + \mathcal{D}_h F_h = 0. \tag{2.53}$$

Remark 2.17. If (2.52) corresponds to (2.37)-(2.38) or (2.41)-(2.42) with $U_h = (cB_h, \boldsymbol{E}_h)$, then Property (i) in Definition 2.16 is consistent with Definition 2.11 or 2.12, see Lemma 2.15.

Remark 2.18. With the notation of Definition 2.11, the first equation from (2.53) is trivial and the second one rewrites as

$$\partial_t \rho_h + \operatorname{div}_h \boldsymbol{J}_h = 0. \tag{2.54}$$

Remark 2.19. Given a semi-discrete scheme of the form (2.37), one could think of *defining* ρ_h from ρ_h^0 and (2.54), but as outlined in Section 2.1 the whole point of charge-conserving schemes is to enforce the stability of the field $(B_h, \boldsymbol{E}_h)$ through that of an approximate charge density ρ_h that is already available as a good (i.e. stable) approximation of the exact charge density. Thus it is important to see (2.54) as a condition to be satisfied by the discrete current density $\boldsymbol{J}_h$.

Equipped with the above definitions we can state a long-time stability result and an error estimate that behaves well on long time ranges.

Theorem 2.20. *Let* (2.37)-(2.38) *be a charge-conserving space discretization of the Maxwell equations in the sense of Def. 2.16. Then for any solution $B_h, \boldsymbol{E}_h$ of the discrete Ampère and Faraday laws* (2.37)*, the discrete Gauss laws* (2.38) *hold for all $t \geq 0$ iff they hold at $t = 0$. Moreover, the following estimate holds for $U_h = (cB_h, \boldsymbol{E}_h)$,*

$$\|U_h(t)\| \leq c_P\Big(\|R_h(t)\| + \|F_h(t)\| + \|\mathcal{A}_h U_h(0)\| + \|F_h(0)\| + \Big\| \int_0^t e^{(t-s)\mathcal{A}_h} \partial_t F_h(s)\,\mathrm{d}s \Big\|\Big) \tag{2.55}$$

where $\mathcal{A}_h := c\left(\begin{smallmatrix} 0 & -\operatorname{curl}_h \\ \mathbf{curl}_h & 0 \end{smallmatrix}\right)$ is the discrete evolution operator, $R_h = ((\iota_h)^* cB_h^0, \varepsilon_0^{-1}\rho_h)^T$ and $F_h = (0, \varepsilon_0^{-1}\boldsymbol{J}_h)^T$ represent the discrete sources and c_P is the constant in the Poincaré estimates (2.40).

If in addition $\mathcal{A}_h$ forms a Gauss-compatible approximation of the exact operator (2.21) *with a mapping Π_h on $\mathcal{V}_h = V_h^1 \times V_h^2$, see Definition 2.3, then the error estimate*

$$\begin{aligned} \|(U_h - \hat{\Pi}_h U)(t)\| \leq c_P\Big(&\|(R_h - \mathcal{D}_h\hat{\Pi}_h U)(t)\| + \|(F_h - \Pi_h F)(t)\| + \|\mathcal{A}_h(U_h - \hat{\Pi}_h U)(0)\| + \|(F_h - \Pi_h F)(0)\| \\ &+ \Big\| \int_0^t e^{(t-s)\mathcal{A}_h} \partial_t (F_h - \Pi_h F)(s)\,\mathrm{d}s \Big\| + \Big\| \int_0^t e^{(t-s)\mathcal{A}_h} \mathcal{A}_h (\hat{\Pi}_h - \Pi_h)\partial_t U(s)\,\mathrm{d}s \Big\|\Big) \end{aligned} \tag{2.56}$$

holds for any exact solution $U = (cB, \boldsymbol{E}) \in C^0([0,T]; \hat{\mathcal{V}})$ of (2.22). *Here $\hat{\Pi}_h : \hat{\mathcal{V}} \to \mathcal{V}_h$ is the auxiliary mapping from Definition 2.3, and c_P is again the constant from* (2.40).

Proof.
Using Lemma 2.15 we know that the composite operators $\mathcal{A}_h$ and $\mathcal{D}_h$ satisfy the key properties (2.11), (2.12) and (2.13). Since $\operatorname{Im}\mathcal{A}_h = (\ker\mathcal{A}_h)^\perp$ by skew-symmetry, this implies that $\mathcal{D}_h\mathcal{A}_h = 0$. Thus, by applying $\mathcal{D}_h$ to the composite form (2.36) of the Maxwell scheme and using the discrete continuity equation (2.53), we find that the discrete Gauss laws

$$\mathcal{D}_h U_h = R_h = \begin{pmatrix} (\iota_h)^* c B_h^0 \\ \varepsilon_0^{-1}\rho_h \end{pmatrix} \tag{2.57}$$

i.e. (2.38), are preserved in time. By computing as in (2.10), using the properties (2.11), (2.12), (2.13) and a discrete Duhamel formula for U_h (together with the contraction properties of $e^{t\mathcal{A}_h}$) we then find

$$\|U_h(t)\| \le c_P\Big(\|R_h(t)\| + \|\mathcal{A}_h U_h(0)\| + \Big\|\int_0^t e^{(t-s)\mathcal{A}_h}\mathcal{A}_h F_h(s)\,\mathrm{d}s\Big\|\Big) \tag{2.58}$$

and the stability estimate (2.55) follows by integrating by parts,

$$\int_0^t e^{(t-s)\mathcal{A}_h}\mathcal{A}_h F_h(s)\,\mathrm{d}s = \int_0^t e^{(t-s)\mathcal{A}_h}\partial_t F_h(s)\,\mathrm{d}s - [e^{(t-s)\mathcal{A}_h}F_h(s)]_0^t. \tag{2.59}$$

To prove the error estimate we observe that, as a consequence of the commuting diagram $\Pi_h\mathcal{A} = \mathcal{A}_h\hat{\Pi}_h$, the error term $\check{U}_h := (U_h - \hat{\Pi}_h U)$ satisfies the discrete Maxwell system

$$\begin{cases} \partial_t\check{U}_h - \mathcal{A}_h\check{U}_h = -\check{F}_h \\ \mathcal{D}_h U_h = \check{R}_h \end{cases} \quad \text{with source terms} \quad \begin{cases} \check{F}_h := (F_h - \Pi_h F) + (\hat{\Pi}_h - \Pi_h)\partial_t U \\ \check{R}_h := R_h - \mathcal{D}_h\hat{\Pi}_h U. \end{cases}$$

Thus, the stability estimate (2.58) applies. By performing an integration by part similar to (2.59) for the source term corresponding to $(F_h - \Pi_h F)$, we arrive at (2.56). ∎

Again we observe that some simpler estimates can be derived from the skew-symmetry of $\mathcal{A}_h$. For instance, using the contraction properties of the semi-group $e^{t\mathcal{A}_h}$ we can infer from (2.56) that

$$\|(U_h - \hat{\Pi}_h U)(t)\| \le c_P\Big(\|(R_h - \mathcal{D}_h\hat{\Pi}_h U)(t)\| + \|(F_h - \Pi_h F)(t)\| + \|\mathcal{A}_h(U_h - \hat{\Pi}_h U)(0)\| + \|(F_h - \Pi_h F)(0)\| + \int_0^t \Big(\|\partial_t(F_h - \Pi_h F)(s)\| + \|\mathcal{A}_h(\hat{\Pi}_h - \Pi_h)\partial_t U(s)\|\Big)\,\mathrm{d}s\Big).$$

holds for any exact solution $U \in \mathcal{C}^0([0,T];\hat{\mathcal{V}})$ of (2.22). Moreover, reasonning as in Corollary 2.7 and Remark 2.8 we can show that (i) the long-time stability holds for almost every time-harmonic solution and (ii) for spectrally correct discretizations no long-time instability is likely to appear for frequencies outside the discrete spectrum of $\mathcal{A}$.

Remark 2.21. As noted above, Theorem 2.20 readily applies to more general models such as the 3D Maxwell system as long as they can be put in the form (2.52).

Applications to specific Maxwell solvers will be described in Sections 3.4 and 4.2 below, as well as in our companion article [21].

3. Conforming elements for the 2D Maxwell system with a strong Ampère law

Although it makes no difference on the continuous problem whether one takes (2.19) or (2.20) for the primal complex, on the discrete level it leads to two different types of Galerkin methods. In this article we describe the first choice which leads to a strong discretization of the Ampère equation with natural boundary conditions. The second choice leading to a strong discrete Faraday equation with essential boundary conditions is dealt with in our companion article [21].

Because the construction of our new non-conforming method relies on a good understanding of the conforming tools, we now verify that the structure of the Finite Element exterior calculus introduced by Arnold, Falk and Winther [2, 3, 4], linking the conforming Galerkin approximations of the different Hilbert spaces perfectly fits in the framework introduced in the previous sections. Specifically, this will allow us to show in Section 3.4 that a standard sequence of Finite Element spaces can be equipped with a Gauss-compatible approximation operator in the sense of Definition 2.3, and in Section 5.1 we will verify that it naturally yields a structure-preserving discretization of Maxwell's equations in the sense of Definition 2.11. Our non-conforming approximation will consist in giving more freedom in the choice of the discrete spaces, in particular to include discontinuous broken spaces, and in carefully choosing the projection operators and discrete differential operators so as to preserve the commuting diagram (2.31) and the exact sequence (2.39).

3.1. **Mesh notations**

We begin by specifying some notations for the mesh elements. We assume that the domain Ω is partitioned by a regular family of conforming simplicial meshes $\mathcal{T}_h$ with maximal triangle diameter h tending to zero. We assume that the triangles in $\mathcal{T}_h$ are numbered with integers $i = 0, \dots \#(\mathcal{T}_h) - 1$, and that the vertices $\mathcal{X}(T) = \{\mathbf{x}_0^T, \mathbf{x}_1^T, \mathbf{x}_2^T\}$ of each triangle $T \in \mathcal{T}_h$ are numbered counterclockwise. We denote the corresponding edges by $\mathcal{E}(T) = \{e_0^T, e_1^T, e_2^T\}$, so that e_k^T and $\mathbf{x}_k^T$ are facing each other. We also let $\boldsymbol{n}_e^T$ be the outward unit vector of T that is normal to e, and $\boldsymbol{\tau}_e^T$ the associated tangent vector obtained by rotating $\boldsymbol{n}_e^T$ through + 90 degrees as illustrated in Figure 3.1. Finally the sets containing all the edges and vertices in the mesh are denoted by

$$\mathcal{E}_h = \cup_{T\in\mathcal{T}_h}\mathcal{E}(T) \qquad \text{and} \qquad \mathcal{X}_h = \cup_{T\in\mathcal{T}_h}\mathcal{X}(T).$$

We then fix an orientation for the edges as follows. For any $e \in \mathcal{E}_h$, we let $T^-(e)$ be the triangle of minimum index for which e is an edge. If e is shared by another triangle we denote the latter by $T^+(e)$. Due to the conformity of the mesh, no more than 2 triangles can have e as an edge. The edge e is then oriented by setting

$$\mathbf{x}_0^e := \mathbf{x}_{k+1}^{T^-(e)}, \quad \mathbf{x}_1^e := \mathbf{x}_{k+2}^{T^-(e)} \qquad \text{where } k \text{ is such that } e = e_k^{T^-(e)} \tag{3.1}$$

(and where for simplicity we have identified $\mathbf{x}_k^{T^-(e)}$ and $\mathbf{x}_{k+3}^{T^-(e)}$). We also set

$$\boldsymbol{n}_e := \boldsymbol{n}_e^{T^-(e)},$$

and observe that if e is an interior edge then we have $\boldsymbol{n}_e = -\boldsymbol{n}_e^{T^+(e)}$.

3.2. **Conforming Finite Elements with a strong Ampère law**

In order to derive finite element schemes with a strong Ampère equation we approximate the non-trivial spaces in the primal sequence (2.19), i.e.,

$$V^1 = H(\mathbf{curl};\Omega) \xrightarrow{d^1=\mathbf{curl}} V^2 = \boldsymbol{H}(\mathrm{div};\Omega) \xrightarrow{d^2=\mathrm{div}} V^3 = L^2(\Omega)$$

by a sequence of discrete spaces $V_h^1 \xrightarrow{d_h^1} V_h^2 \xrightarrow{d_h^2} V_h^3$. If we opt for a conforming sequence, i.e., such that $V_h^l \subset V^l$, then we can define d_h^l as the restriction of d^l. Several options are then possible for these spaces. Here we shall follow a common strategy (see, e.g., [1]) where the discrete spaces V_h^l are known as the continuous Finite Element space, the Raviart-Thomas Finite Element space and the

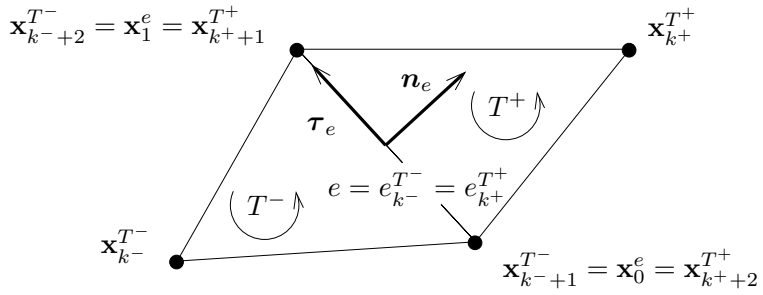

FIGURE 3.1. Notations for vertices and edges in the triangles: here $T^\pm$ stand for $T^\pm(e)$, and $k^\pm$ are the local indices of e in these respective triangles. The unit vectors $\boldsymbol{n}_e$ (normal to e) and $\boldsymbol{\tau}_e$ (tangent to e) are oriented with respect to $T^-(e)$, see details in the text.

discontinuous Galerkin Finite Element space. Specifically, given an integer degree $p \geq 1$ we take

$$V_h^1 := \mathcal{L}_p(\Omega, \mathcal{T}_h) \xrightarrow{d_h^1 := \mathbf{curl}\,|_{V_h^1}} V_h^2 := \boldsymbol{\mathcal{RT}}_{p-1}(\Omega, \mathcal{T}_h) \xrightarrow{d_h^2 := \mathrm{div}\,|_{V_h^2}} V_h^3 := \mathbb{P}_{p-1}(\mathcal{T}_h) \tag{3.2}$$

where

$$\mathbb{P}_{p-1}(\mathcal{T}_h) := \{v \in L^2(\Omega) : v|_T \in \mathbb{P}_{p-1}(T),\ T \in \mathcal{T}_h\} \tag{3.3}$$

denotes the space of piecewise polynomials of maximal degree $p-1$ on the triangulation $\mathcal{T}_h$,

$$\mathcal{L}_p(\Omega, \mathcal{T}_h) := \mathbb{P}_p(\mathcal{T}_h) \cap H(\mathbf{curl}; \Omega) = \mathbb{P}_p(\mathcal{T}_h) \cap \mathcal{C}(\Omega) \tag{3.4}$$

corresponds to the continuous "Lagrange" elements of maximal degree p and finally

$$\boldsymbol{\mathcal{RT}}_{p-1}(\Omega, \mathcal{T}_h) := \boldsymbol{\mathcal{RT}}_{p-1}(\mathcal{T}_h) \cap \boldsymbol{H}(\mathrm{div}; \Omega) \quad \text{with} \quad \boldsymbol{\mathcal{RT}}_{p-1}(T) := \mathbb{P}_{p-1}(T)^2 + \binom{x}{y}\mathbb{P}_{p-1}(T) \tag{3.5}$$

is the Raviart-Thomas Finite Element space of order $p-1$ (thus of maximal degree p), see e.g., [63] or [8].

Remark 3.1. To be conforming in $\boldsymbol{H}(\mathrm{div}; \Omega)$, the piecewise polynomial space V_h^2 must be composed of vector fields that have no normal discontinuities on the edges of the mesh, in the sense that for any $\boldsymbol{v} \in V_h^2$ the normal trace $\boldsymbol{n}_e \cdot \boldsymbol{v}$ on an edge e must be the same when defined either from $T^-(e)$ or from $T^+(e)$. In particular, every basis of V_h^2 must contain some vector fields supported on two adjacent cells at least.

For the sake of completeness we recall the following well-known result which will be central to our analysis.

Lemma 3.2. *The following sequence is exact, in the sense that the range of each operator coincides with the kernel of the following operator,*

$$\mathbb{R} \xrightarrow{\iota} \mathcal{L}_p(\Omega, \mathcal{T}_h) \xrightarrow{d_h^1 = \mathbf{curl}} \boldsymbol{\mathcal{RT}}_{p-1}(\Omega, \mathcal{T}_h) \xrightarrow{d_h^2 = \mathrm{div}} \mathbb{P}_{p-1}(\mathcal{T}_h) \xrightarrow{0} \{0\}$$

where we remind that ι is the canonical injection in $L^2(\Omega)$.

Proof. The arguments are standard (see, e.g., [11, 40, 55]) and we recall them here for completeness. The first claimed equality ($\ker d_h^1 = \mathbb{R}$) is obvious since d_h^1 coincides with the 2D **curl** operator on V_h^1. The second claimed equality is

$$\ker d_h^2 = d_h^1 V_h^1$$

i.e., $\ker(\operatorname{div}|_{V_h^2}) = \mathbf{curl}\, V_h^1$. To verify it, write any $\boldsymbol{u} \in \boldsymbol{\mathcal{RT}}_{p-1}$ as $\boldsymbol{u} = \boldsymbol{v} + \binom{x}{y}\tilde{v}$ with $\boldsymbol{v} \in \mathbb{P}_{p-1}^2$ and $\tilde{v}$ a homogeneous polynomial (possibly zero) of total degree $p-1$, so that $\operatorname{div}\boldsymbol{u} = \operatorname{div}\boldsymbol{v} + (p+1)\tilde{v}$. Now, as $\operatorname{div}\boldsymbol{v}$ clearly belongs to $\mathbb{P}_{p-2}$, $\operatorname{div}\boldsymbol{u} = 0$ yields $\tilde{v} = 0$ and hence $\boldsymbol{u} \in \mathbb{P}_{p-1}^2$. Using this observation with the continuous exact sequence property, we find $\boldsymbol{u} = \mathbf{curl}\,\phi$ for some $\phi \in \mathbb{P}_p$, hence the result. Finally the last claimed equality is

$$V_h^3 = d_h^2 V_h^2$$

i.e., $\mathbb{P}_{p-1}(\mathcal{T}_h) = \operatorname{div} V_h^2$, and it is easily proven by counting the dimensions of the different discrete spaces, using Euler's formula $\#(\mathcal{X}_h) - \#(\mathcal{E}_h) + \#(\mathcal{T}_h) = 1$. ∎

Based on the above spaces, a standard conforming Finite Element method consists in computing the unique solution $(B_h, \boldsymbol{E}_h) \in \mathcal{C}^0([0,T]; V_h^1 \times V_h^2)$ to

$$\begin{cases} \langle \partial_t B_h, \varphi^1\rangle + \langle \boldsymbol{E}_h, \mathbf{curl}\,\varphi^1\rangle = 0 & \varphi^1 \in V_h^1 \subset H(\mathbf{curl};\Omega) \\ \langle \partial_t \boldsymbol{E}_h, \boldsymbol{\varphi}^2\rangle - c^2\langle \mathbf{curl}\, B_h, \boldsymbol{\varphi}^2\rangle = -\frac{1}{\varepsilon_0}\langle \boldsymbol{J}_h, \boldsymbol{\varphi}^2\rangle & \boldsymbol{\varphi}^2 \in V_h^2 \subset \boldsymbol{H}(\operatorname{div};\Omega) \end{cases} \tag{3.6}$$

where $\boldsymbol{J}_h \in \mathcal{C}^0([0,T]; V_h^2)$ represents an approximation of the given current density $\boldsymbol{J}$ and $\langle\cdot,\cdot\rangle$ stands for the scalar product in $L^2(\Omega)$. Note that using the embedding $\mathbf{curl}\, V_h^1 \subset V_h^2$ the second equation amounts to

$$\partial_t \boldsymbol{E}_h - c^2\,\mathbf{curl}\, B_h = -\tfrac{1}{\varepsilon_0}\boldsymbol{J}_h \qquad (\text{in } V_h^2) \tag{3.7}$$

which justifies our "strong Ampère" terminology.

This space discretization has been studied in Ref. [1, 52] where the source term $\boldsymbol{J}$ is approximated with a standard orthogonal projection on V_h^2, leading to define $\boldsymbol{J}_h$ by $\langle \boldsymbol{J}_h, \boldsymbol{\varphi}^2\rangle = \langle \boldsymbol{J}, \boldsymbol{\varphi}^2\rangle$ for $\boldsymbol{\varphi}^2 \in V_h^2$. In order to obtain a compatible scheme we propose instead to approximate the source with a Raviart-Thomas interpolation on the space V_h^2, see Theorem 3.5 below. To this end we first recall how this projection is defined (see Equation (3.15) below) and what are its basic commutation properties. We note that at the lowest order, the resulting formulation corresponds to the D/H formulation outlined in Ref. [69], in the language of discrete differential forms.

3.3. **Projection operators and commuting diagram properties**

In the conforming Finite Element case the projection operators and commuting diagram properties have been discussed and described in a series of papers by Arnold, Falk and Winther on what they call the Finite Element Exterior Calculus (FEEC) [2, 3, 4]. For the discrete spaces (3.3)-(3.5) introduced in the previous section, the commuting diagram properties are obtained when using the so-called canonical projection operators, which are introduced in [2, p. 56]. Their main feature is to separate, for the 2D case, vertex degrees of freedom, edge degrees of freedom and face degrees of freedom. The first projection in the sequence, corresponding to projection of 0-forms has all three types, the second corresponding to 1-forms has no vertex degrees of freedom and the third corresponding to 2-forms has only face (or volume) based degrees of freedom, and thus simply corresponds to an orthogonal projection in L^2. This can be represented with the following commuting diagram:

$$\begin{array}{ccccc} H^2(\Omega) & \xrightarrow{\mathbf{curl}} & H^1(\Omega)^2 & \xrightarrow{\operatorname{div}} & L^2(\Omega) \\ \downarrow{\scriptstyle \pi_h^{\mathbf{curl}}} & & \downarrow{\scriptstyle \pi_h^{\operatorname{div}}} & & \downarrow{\scriptstyle P_{V_h^3}} \\ V_h^1 & \xrightarrow{\mathbf{curl}} & V_h^2 & \xrightarrow{\operatorname{div}} & V_h^3. \end{array} \tag{3.8}$$

In order to avoid the formalism of differential forms, which is not necessary for our application, we shall recall the canonical projections and discrete spaces and justify the commuting diagram with elementary tools, see Equations (3.17) and (3.19) below.

On the **curl**-conforming space V_h^1 the canonical projection of Arnold, Falk and Winther is the following projection, which can also be seen as a restriction of the 3D projection of Nédélec [61]. Given an arbitrary triangle T, we first define the following sets of moments (or degrees of freedoms),

$$\begin{cases} \mathcal{M}_h^1(T,u) := \{\int_T u\varphi : \varphi \in \mathbb{P}_{p-3}(T)\} & \\ \mathcal{M}_h^1(e,u) := \{\int_e u\,\varphi : \varphi \in \mathbb{P}_{p-2}(e)\} & \text{for every edge } e \in \mathcal{E}(T) \\ \mathcal{M}_h^1(\mathbf{x},u) := \{u(\mathbf{x})\} & \text{for every vertex } \mathbf{x} \in \mathcal{X}(T). \end{cases} \tag{3.9}$$

Lemma 3.3. *The above degrees of freedom are unisolvent on $\mathbb{P}_p(T)$ and* **curl***-conforming.*

The proof uses standard arguments [55] and is recalled in [20].

It is then possible to define a local projection r_T^1 on $\mathbb{P}_p(T)$ by the relations

$$\begin{cases} \mathcal{M}_h^1(T, r_T^1 u - u) = \{0\} & \\ \mathcal{M}_h^1(e, r_T^1 u - u) = \{0\}, & e \in \mathcal{E}(T) \\ \mathcal{M}_h^1(\mathbf{x}, r_T^1 u - u) = \{0\}, & \mathbf{x} \in \mathcal{X}(T). \end{cases}$$

A global projection $\pi_h^{\mathbf{curl}} : \mathcal{C}^0(\Omega) \to H(\mathbf{curl};\Omega) \cap \mathbb{P}_p(\mathcal{T}_h)$ is then obtained by stitching together the individual pieces, i.e., by setting

$$\pi_h^{\mathbf{curl}} u := \sum_{T\in\mathcal{T}_h} \mathbb{1}_T r_T^1 u. \tag{3.10}$$

Using standard arguments (namely, the use of a reference element $\hat{T}$ and the compact embedding of $H^2(\hat{T})$ on $L^\infty(\hat{T})$), one can verify that the following error estimate holds,

$$\|\pi_h^{\mathbf{curl}} u - u\| \le c h^m |u|_m, \qquad 2 \le m \le p+1. \tag{3.11}$$

When designing non-conforming approximations based on broken spaces in Section 4.1 it will be convenient to follow [31] and use a basis for V_h^1 that is dual to the above degrees of freedom. The construction of such a basis is very classical in Finite Elements and can be summarized as follows. Given some bases $q_{e,i}$, $i = 1,\dots p-1$ for the edge polynomials $\mathbb{P}_{p-2}(e)$, $e \in \mathcal{E}_h$, and some others $q_{T,i}$, $i = 1,\dots,\frac{(p-2)(p-1)}{2}$ for the "volume" polynomials $\mathbb{P}_{p-3}(T)$, $T \in \mathcal{T}_h$, we span the moment spaces listed in (3.9) with the degrees of freedom

$$\begin{cases} \sigma_{T,i}^1(u) = \int_T q_{T,i} u, & T \in \mathcal{T}_h,\ i = 1,\dots,\frac{(p-2)(p-1)}{2} \\ \sigma_{e,i}^1(u) = \int_e q_{e,i} u, & e \in \mathcal{E}_h,\ i = 1,\dots,p-1 \\ \sigma_{\mathbf{x}}^1(u) = u(\mathbf{x}), & \mathbf{x} \in \mathcal{X}_h. \end{cases} \tag{3.12}$$

The following is then guaranteed by Lemma 3.3: First, $\mathbb{P}_p(T)$ admits a unique basis $\varphi_\lambda^{1,T}$ with indices in

$$\Lambda^1(T) := \Lambda^1_{\text{vol}}(T) \cup \Lambda^1_{\text{edge}}(T) \cup \Lambda^1_{\text{vertex}}(T) \quad \text{where} \quad \begin{cases} \Lambda^1_{\text{vol}}(T) := \{(T,i) : i = 1,\dots,\frac{(p-2)(p-1)}{2}\} \\ \Lambda^1_{\text{edge}}(T) := \{(e,i) : e \in \mathcal{E}(T), i = 1,\dots,p-1\} \\ \Lambda^1_{\text{vertex}}(T) := \mathcal{X}(T) \end{cases}$$

that is dual to the associated degrees of freedom, in the sense that $\sigma_\gamma^1(\varphi_\lambda^{1,T}) = \delta_{\gamma,\lambda}$ holds for $\gamma,\lambda \in \Lambda^1(T)$. Second, if we set $\varphi_\lambda^{1,T} := 0$ for $\lambda \in \Lambda_h^1 \setminus \Lambda^1(T)$ with $\Lambda_h^1 := \cup_{T\in\mathcal{T}_h}\Lambda^1(T)$ and if we extend $\varphi_\lambda^{1,T}$ by 0 outside T for $\lambda \in \Lambda^1(T)$, then the piecewise polynomials

$$\varphi_\lambda^1 := \sum_{T\in\mathcal{T}_h} \mathbb{1}_T \varphi_\lambda^{1,T} = \sum_{T\in\mathcal{T}_h} \varphi_\lambda^{1,T} \tag{3.13}$$

are continuous and they form a basis for the global space V_h^1 that is dual to the associated degrees of freedom in the sense that $\sigma_\gamma^1(\varphi_\lambda^1) = \delta_{\gamma,\lambda}$ for all $\gamma,\lambda \in \Lambda_h^1$. Moreover, if the polynomials $q_{e,i}$ and

$q_{T,i}$ involved in (3.12) are defined as suitable affine maps of polynomial bases defined on a reference element, the resulting local basis functions $\varphi_\lambda^{1,T}$ will also correspond to affine maps of the associated reference basis. As a result, if the mesh $\mathcal{T}_h$ is shape regular in the standard sense of, e.g., [35, Def. I-A.2], it is possible to ask for normalized local basis functions satisfying, e.g.,

$$\|\varphi_\lambda^{1,T}\| \sim 1 \qquad \text{for } \ T \in \mathcal{T}_h,\ \lambda \in \Lambda^1(T). \tag{3.14}$$

The second canonical projection in the sequence is the standard Raviart-Thomas interpolation. Let us recall how it is defined. The usual degrees of freedom for the finite element space $V_h^2 = \boldsymbol{\mathcal{RT}}_{p-1}(\Omega, \mathcal{T}_h)$ read (see, e.g., [35] or [8, Sec. 2.3.1 and Ex. 2.5.3])

$$\begin{cases} \mathcal{M}_h^2(T, \boldsymbol{v}) := \{\int_T \boldsymbol{v}\cdot\boldsymbol{\varphi} : \boldsymbol{\varphi} \in \mathbb{P}_{p-2}(T)^2\} & \text{for every triangle } T \in \mathcal{T}_h, \\ \mathcal{M}_h^2(e, \boldsymbol{v}) := \{\int_e (\boldsymbol{n}_e\cdot\boldsymbol{v})\,\varphi : \varphi \in \mathbb{P}_{p-1}(e)\} & \text{for every edge } e \in \mathcal{E}_h. \end{cases}$$

The Raviart-Thomas finite element interpolation

$$\pi_h^{\mathrm{div}} : H^1(\Omega)^2 \to V_h^2 := \boldsymbol{\mathcal{RT}}_{p-1}(\Omega, \mathcal{T}_h)$$

see (3.5), is then defined by the relations

$$\mathcal{M}_h^2(T, \pi_h^{\mathrm{div}}\boldsymbol{v} - \boldsymbol{v}) = \{0\}, \quad T \in \mathcal{T}_h \qquad \text{and} \qquad \mathcal{M}_h^2(e, \pi_h^{\mathrm{div}}\boldsymbol{v} - \boldsymbol{v}) = \{0\}, \quad e \in \mathcal{E}_h \tag{3.15}$$

and classical arguments show that it satisfies the following error estimate (see, e.g., [8, Prop. (2.5.4)]),

$$\|\pi_h^{\mathrm{div}}\boldsymbol{v} - \boldsymbol{v}\| \le ch^m|\boldsymbol{v}|_m, \qquad 1 \le m \le p. \tag{3.16}$$

Moreover, as is well known (see, e.g., [8, Eq. (7.1.27)]) and easily checked using integration by parts, π_h^{div} satisfies a commuting diagram property,

$$\operatorname{div}\pi_h^{\mathrm{div}}\boldsymbol{v} = P_{V_h^3}\operatorname{div}\boldsymbol{v}, \qquad \boldsymbol{v} \in H^1(\Omega)^2 \tag{3.17}$$

where $P_{V_h^3}$ is the L^2 projection on the discontinuous space $V_h^3 = \mathbb{P}_{p-1}(\mathcal{T}_h)$. Note that this property readily gives an additional error estimate, namely

$$\|\operatorname{div}(\pi_h^{\mathrm{div}}\boldsymbol{v} - \boldsymbol{v})\| \le ch^m|\operatorname{div}\boldsymbol{v}|_m, \qquad 0 \le m \le p\ . \tag{3.18}$$

We also verify that $\pi_h^{\mathbf{curl}}$ defined by (3.10) satisfies a commuting diagram property.

Lemma 3.4. *We have*

$$\mathbf{curl}\,\pi_h^{\mathbf{curl}}u = \pi_h^{\mathrm{div}}\,\mathbf{curl}\,u, \qquad u \in \mathcal{C}^0(\Omega). \tag{3.19}$$

Again the proof follows from standard computations using the above definition of the degrees of freedom, it is given for completeness in [20].

3.4. **Gauss-compatibility of the conforming FEM-Ampère scheme**

In compact form, the conforming FEM-Ampère scheme (3.6) reads $\partial_t U_h - \mathcal{A}_h U_h = -F_h = -\Pi_h F$ with $U_h = (cB_h, \boldsymbol{E}_h)^T$, $F = (0, \varepsilon_0^{-1}\boldsymbol{J})^T$ and a composite curl operator defined on $\mathcal{V}_h := V_h^1 \times V_h^2$ by

$$\mathcal{A}_h := c\begin{pmatrix} 0 & -\operatorname{curl}_h \\ \mathbf{curl}_h & 0 \end{pmatrix} \qquad \text{with} \qquad \begin{cases} \mathbf{curl}_h := \mathbf{curl}\,|_{V_h^1} : V_h^1 \to V_h^2 \\ \operatorname{curl}_h := (\mathbf{curl}_h)^* : V_h^2 \to V_h^1. \end{cases} \tag{3.20}$$

Following Definition 2.3 and considering source and auxiliary approximation operators of the form

$$\Pi_h = \begin{pmatrix} \pi_h^1 & 0 \\ 0 & \pi_h^2 \end{pmatrix} \qquad \text{and} \qquad \hat{\Pi}_h = \begin{pmatrix} \hat{\pi}_h^1 & 0 \\ 0 & \hat{\pi}_h^2 \end{pmatrix} \tag{3.21}$$

we then see that this scheme is Gauss-compatible on some product space $\hat{V}^1 \times \hat{V}^2$ if for $l = 1, 2$ we can find approximation operators π_h^l and $\hat{\pi}_h^l$ mapping on V_h^l, such that

$$\pi_h^2 \mathbf{curl}\, u = \mathbf{curl}\, \hat{\pi}_h^1 u, \qquad u \in \hat{V}^1 \tag{3.22}$$

and

$$\pi_h^1 \operatorname{curl} \boldsymbol{u} = (\mathbf{curl}_h)^* \hat{\pi}_h^2 \boldsymbol{u}, \qquad \boldsymbol{u} \in \hat{V}^2. \tag{3.23}$$

Note that these relations read $\pi_h^2 d^1 u = d_h^1 \hat{\pi}_h^1 u$ and $\pi_h^1 (d^1)^* \boldsymbol{u} = (d_h^1)^* \hat{\pi}_h^2 \boldsymbol{u}$ with the notations of Section 2.2 and 3.2.

Theorem 3.5. *The conforming FEM-Ampère scheme* (3.6) *associated with the Raviart-Thomas interpolation* (3.15) *for the current, namely*

$$\pi_h^2 := \pi_h^{\mathrm{div}} : H^1(\Omega)^2 \to V_h^2 = \boldsymbol{\mathcal{RT}}_{p-1}(\Omega, \mathcal{T}_h),$$

is Gauss-compatible on the product space

$$\hat{V}^1 \times \hat{V}^2 := \mathcal{C}^0(\Omega) \times V_2^*$$

where $V_2^* = \boldsymbol{H}_0(\mathrm{curl}; \Omega)$*, see Section 2.2. Specifically, Equation* (3.22) *holds with* $\hat{\pi}_h^1 := \pi_h^{\mathbf{curl}}$ *defined in* (3.10) *and Equation* (3.23) *holds with the* L^2*-projections* $\pi_h^1 := P_{V_h^1}$ *and* $\hat{\pi}_h^2 := P_{V_h^2}$*. Moreover, these mappings satisfy*

$$\|\hat{\pi}_h^1 u - u\| \lesssim h^m |u|_m, \qquad 2 \le m \le p+1 \tag{3.24}$$

$$\|\hat{\pi}_h^2 \boldsymbol{u} - \boldsymbol{u}\| \lesssim h^m |\boldsymbol{u}|_m, \qquad 0 \le m \le p \tag{3.25}$$

$$\|\pi_h^1 u - u\| \lesssim h^m |u|_m, \qquad 0 \le m \le p+1 \tag{3.26}$$

$$\|\pi_h^2 \boldsymbol{u} - \boldsymbol{u}\| \lesssim h^m |\boldsymbol{u}|_m, \qquad 1 \le m \le p. \tag{3.27}$$

Proof. The fact that Relation (3.22) holds with $\pi_h^2 = \pi_h^{\mathrm{div}}$ and $\hat{\pi}_h^1 = \pi_h^{\mathbf{curl}}$ follows from Lemma 3.4. As for (3.23), we can test it against an arbitrary $v \in V_h^1 \subset V^1$ since both sides belong to V_h^1 by construction. Using the definition of the various operators we compute

$$\langle P_{V_h^1} (d^1)^* \boldsymbol{u}, v \rangle = \langle (d^1)^* \boldsymbol{u}, v \rangle = \langle \boldsymbol{u}, d^1 v \rangle = \langle \boldsymbol{u}, d_h^1 v \rangle = \langle P_{V_h^2} \boldsymbol{u}, d_h^1 v \rangle = \langle (d_h^1)^* P_{V_h^2} \boldsymbol{u}, v \rangle,$$

which proves (3.23). Estimates (3.25) and (3.26) are standard for L^2 projections, whereas (3.24) and (3.27) are just (3.11) and (3.16), respectively. ∎

If one is solving the Maxwell equations with exact sources, Theorem 2.5 applies and gives the following a priori estimate.

Corollary 3.6. *Let* $(B, \boldsymbol{E})$ *be the exact solution to the Maxwell system* (2.22)*. The semi-discrete solution to the FEM-Ampère scheme* (3.6) *coupled with the Raviart-Thomas interpolation* (3.15) *for the current satisfies*

$$\begin{aligned}\|(B - B_h)(t)\| + \|(\boldsymbol{E} - \boldsymbol{E}_h)(t)\| \lesssim{}& \|B_h(0) - \hat{\pi}_h^1 B(0)\| + \|\boldsymbol{E}_h(0) - \hat{\pi}_h^2 \boldsymbol{E}(0)\| \\ &+ h^m \Big(|B(0)|_m + \int_0^t |\partial_t B(s)|_m \, \mathrm{d}s \Big) + h^{m'} \Big(|\boldsymbol{E}(0)|_{m'} + \int_0^t |\partial_t \boldsymbol{E}(s)|_{m'} \, \mathrm{d}s \Big)\end{aligned}$$

for $2 \le m \le p+1$*,* $1 \le m' \le p$*, and with a constant independent of* h *and* t*.*

Remark 3.7. In Section 6 we will see that approximating the source with an L^2 projection operator does not give a long-time stable scheme. In addition to yield better stability properties, the use of a Raviart-Thomas interpolation rather than an L^2 projection to define the approximate source $\boldsymbol{J}_h$ has the advantage to result in local computations.

Remark 3.8. In the case of approximate sources, one must resort to the analysis developped in Section 2.4 to be able to derive long-time stability estimates. This will be done in Section 5.1 by showing that the FEM-Ampère scheme (3.6) is naturally structure-preserving.

Remark 3.9. Using the Raviart-Thomas interpolation (3.15) requires a smooth ($H^1(\Omega)^2$) current density, and we note that the charge-conserving deposition method described in [69], for a conforming Finite Element scheme corresponding to a low-order version of the strong Ampère scheme expressed in terms of discrete differential forms, also involves some smoothing of the particles. For source terms with less regularity one could think of using the local smoothed projections constructed in [33] following [24, 65, 2, 25], indeed they are well-defined on minimal regularity spaces (e.g. $\boldsymbol{H}(\mathrm{div};\Omega)$ for $\boldsymbol{J}$) and they satisfy the desired commuting diagram (3.22). We note however that their implementation might be delicate in practice.

4. Discontinuous elements for the 2D Maxwell system with a strong Ampère law

Because of its weak formulation, discretizing in time the Faraday law from (3.6) requires to invert a mass matrix associated with the space V_h^1, and due to the **curl**-conformity of the latter space the resulting inversion can not be performed locally. This can of course become a computational burden when the meshes become very fine and when parallel algorithms come into play. For this reason we propose a non-conforming method where the solution is approximated in the fully discontinuous space

$$\tilde{V}_h^1 := \mathbb{P}_p(\mathcal{T}_h) \not\subset V^1 = H(\mathbf{curl};\Omega),$$

see (3.3). Although the common way for designing non-conforming discretizations is to follow the discontinuous Galerkin methodology (see e.g. [34, 43]), in this work we aim at preserving a strong Ampère equation like (3.7). For this purpose we follow a different path and apply to the 2D setting the ideas of the Conga discretization proposed and studied in [22] for the 3D Maxwell system (the name standing for "Conforming/Non-conforming Galerkin"). In particular our non-conforming discretization will be derived from the conforming one (3.2), and we note that this restricts the analysis to positive degrees $p \geq 1$.

As we did for the conforming case, and following our 3D study [22], we will show that this non-conforming discretization can be equipped with a Gauss-compatible approximation operator in the sense of Definition 2.3. In Section 5.2 we will extend this analysis by further verifying that it is essentially a structure-preserving discretization of Maxwell's equations in the sense of Definition 2.11, once associated with a nonstandard discrete divergence.

4.1. Non-conforming "Conga" discretization

To extend the conforming method (3.6) on the non-conforming space $\tilde{V}_h^1$ we consider a smoothing projection

$$\mathcal{P}_h^1 : L^2(\Omega)^2 \to V_h^1 \tag{4.1}$$

(which is not required to satisfy a commuting diagram) and we define the associated Conga approximation $(B_h, \boldsymbol{E}_h) \in \mathcal{C}^0([0,T];\tilde{V}_h^1 \times V_h^2)$ by the system

$$\begin{cases} \langle \partial_t B_h, \tilde{\varphi}^1 \rangle + \langle \boldsymbol{E}_h, \mathbf{curl}\, \mathcal{P}_h^1 \tilde{\varphi}^1 \rangle = 0 & \tilde{\varphi}^1 \in \tilde{V}_h^1 \not\subset H(\mathbf{curl};\Omega) \\ \partial_t \boldsymbol{E}_h - c^2\, \mathbf{curl}\, \mathcal{P}_h^1 B_h = -\frac{1}{\varepsilon_0} \boldsymbol{J}_h & \text{in } V_h^2 \subset \boldsymbol{H}(\mathrm{div};\Omega) \end{cases} \tag{4.2}$$

where again $\boldsymbol{J}_h$ denotes an appropriate approximation of the current density $\boldsymbol{J}$. Below we will see that Gauss-compatible and charge-conserving schemes are obtained with Raviart-Thomas interpolations, as in the conforming case.

For the smoothing projection $\mathcal{P}_h^1$ one may think of using the L^2 projection on the conforming space V_h^1, but this would have the downside of requiring to invert a V_h^1 mass matrix, a global computation that we precisely whish to avoid. Similarly as in [22] we thus use an averaging procedure based on the canonical degrees of freedom for the **curl**-conforming space V_h^1, here (3.9). To obtain a stable projection in L^2 we can recycle the elegant construction proposed in [31], where on each mesh triangle T the authors use the local basis that is dual to the broken basis functions built in Section 3.3, namely the basis $\psi_\lambda^{1,T}$, $\lambda \in \Lambda^1(T)$, of $\mathbb{P}_p(T)$ that is defined by the relations

$$\langle \psi_\lambda^{1,T}, \varphi_\gamma^{1,T} \rangle = \sigma_\lambda^1(\varphi_\gamma^{1,T}|_T) = \delta_{\lambda,\gamma} \quad \text{for} \quad \lambda, \gamma \in \Lambda^1(T). \tag{4.3}$$

A convenient projection operator $\mathcal{P}_h^1 : L^2(\Omega) \to V_h^1$ is then defined by

$$\mathcal{P}_h^1 u := \sum_{T \in \mathcal{T}_h} \sum_{\lambda \in \Lambda^1(T)} \frac{\int \varphi_\lambda^{1,T}}{\int \varphi_\lambda^1} \langle u, \psi_\lambda^{1,T} \rangle \varphi_\lambda^1. \tag{4.4}$$

We note that this is indeed a projection thanks to $\varphi_\lambda^1 = \sum_T \varphi_\lambda^{1,T}$, see (3.13), and on $\tilde{V}_h^1$ it amounts to averaging the broken version of the degrees of freedom (3.12). Indeed, decomposing $\tilde{u} \in \tilde{V}_h^1$ as $\tilde{u} = \sum_{T \in \mathcal{T}_h} \sum_{\lambda \in \Lambda^1(T)} c_\lambda^T \varphi_\lambda^{1,T}$ we infer from the local duality (4.3) that $c_\lambda^T = \sigma_\gamma^1(\tilde{u}|_T)$. Using the duality relation (3.12) we then find

$$\sigma_\gamma^1(\mathcal{P}_h^1 \tilde{u}) = \sigma_\gamma^1 \left(\sum_{T \in \mathcal{T}_h} \sum_{\lambda \in \Lambda^1(T)} \frac{\int \varphi_\lambda^{1,T}}{\int \varphi_\lambda^1} c_\lambda^T \varphi_\lambda^1 \right) = \frac{\sum_{T \in \mathcal{T}_h} \sigma_\gamma^1(\tilde{u}|_T) \int \varphi_\gamma^{1,T}}{\int \varphi_\gamma^1} \qquad \text{for} \quad \gamma \in \Lambda_h^1, \tag{4.5}$$

which is indeed an average since $\varphi_\gamma^1 = \sum_T \varphi_\gamma^{1,T}$.

Remark 4.1. The projection (4.4) slightly differs from the one constructed in [31] where the average is unweighted. Here the choice of the weights allows to preserve the first moments of the functions. Indeed, by writing $\mathbb{1}_\Omega = \sum_{T,\lambda} c_\lambda^T \psi_\lambda^{1,T}$ and integrating the latter against an arbitrary $\varphi_\lambda^{1,T}$ yields $c_\lambda^T = \int \varphi_\lambda^{1,T}$. Therefore,

$$\int \mathcal{P}_h^1 u = \sum_{T \in \mathcal{T}_h} \sum_{\lambda \in \Lambda^1(T)} \int \varphi_\lambda^{1,T} \langle u, \psi_\lambda^{1,T} \rangle = \langle u, \sum_{T \in \mathcal{T}_h} \sum_{\lambda \in \Lambda^1(T)} \psi_\lambda^{1,T} \int \varphi_\lambda^{1,T} \rangle = \langle u, \mathbb{1}_\Omega \rangle = \int u \tag{4.6}$$

holds for all $u \in L^2(\Omega)$.

Just as the basis functions $\varphi_\lambda^{1,T}$ can be obtained as affine maps of reference basis functions with an L^2 normalization (3.14), it is possible to design the dual basis functions with the same property,

$$\|\psi_\lambda^{1,T}\| \sim 1 \qquad \text{for} \quad T \in \mathcal{T}_h, \ \lambda \in \Lambda^1(T). \tag{4.7}$$

In particular it is easily seen that $\mathcal{P}_h^1$ is locally bounded in L^2, and since it is a projection on V_h^1 it satisfies

$$\|(I - \mathcal{P}_h^1)u\| \le C h^m |u|_m, \qquad 0 \le m \le p+1 \tag{4.8}$$

with a constant independent of h. In the analysis of the structure-preserving Conga scheme, an important tool is the adjoint operator $(\mathcal{P}_h^1)^*$ which is bounded on L^2 like $\mathcal{P}_h^1$, and has the form

$$(\mathcal{P}_h^1)^* u = \sum_{T \in \mathcal{T}_h} \sum_{\lambda \in \Lambda^1(T)} \frac{\int_T \varphi_\lambda^{1,T}}{\int \varphi_\lambda^1} \langle u, \varphi_\lambda^1 \rangle \psi_\lambda^{1,T}. \tag{4.9}$$

Lemma 4.2. *The operator $(\mathcal{P}_h^1)^*$ maps on $\tilde{V}_h^1$, it is locally bounded in L^2 and it preserves the piecewise polynomials of $\mathbb{P}_{p-3}(\mathcal{T}_h)$ as well as the constants. In particular, if the mesh $\mathcal{T}_h$ is shape regular we have*

$$\|(I - (\mathcal{P}_h^1)^*)u\| \le C h^m |u|_m, \qquad 0 \le m \le \max(1, p-2) \tag{4.10}$$

with a constant independent of h.

Proof. The fact that $(\mathcal{P}_h^1)^*$ maps on $\tilde{V}_h^1$ is a direct consequence of the definition $\tilde{V}_h^1 = \mathbb{P}_p(\mathcal{T}_h)$, and the local L^2 bound is easily derived using the localized supports of the basis functions φ_λ^1 and the normalization of the primal $\varphi_\lambda^{1,T}$'s and the dual $\psi_\lambda^{1,T}$'s, see (3.14) and (4.7). The fact that $(\mathcal{P}_h^1)^*$ preserves the constants follows from (4.6). Finally to show that $(\mathcal{P}_h^1)^*$ preserve the piecewise polynomials of $\mathbb{P}_{p-3}(\mathcal{T}_h)$, we observe that due to the form of the degrees of freedom of volume type in (3.9), the polynomials $\psi_\lambda^{1,T}$, $\lambda \in \Lambda^1_{\rm vol}(T)$ are in fact of degree not greater than $p-3$ and they form a basis of $\mathbb{P}_{p-3}(T)$ (actually they coincide with the polynomials $q_{T,i}$ in (3.12)). Since the associated primal basis functions φ_λ^1 vanish outside T, they satisfy $\varphi_\lambda^1 = \varphi_\lambda^{1,T}$ and it is easily seen that $(\mathcal{P}_h^1)^*\psi_\lambda^{1,T} = \psi_\lambda^{1,T}$ for all $\lambda \in \Lambda^1_{\rm vol}(T)$. Estimate (4.10) is then a straightforward consequence of these properties and the Bramble-Hilbert Lemma. Note that the preservation of global constants is enough for the first-order estimate ($m=1$): indeed letting Ω_T be the union of the cells which boundary intersects that of T and writing $\bar{u} = |\Omega_T|^{-1}\int_{\Omega_T} u$, we infer from the locality of $(\mathcal{P}_h^1)^*$, see (4.9), that
$\|(I-(\mathcal{P}_h^1)^*)u\|_{L^2(T)} \le \|u-\bar{u}\|_{L^2(T)} + \|(\mathcal{P}_h^1)^*(u-\bar{u})\|_{L^2(T)} \le (1+\|(\mathcal{P}_h^1)^*\|)\|u-\bar{u}\|_{L^2(\Omega_T)} \le Ch|u|_{H^1(\Omega_T)}$
and the global estimate follows from the regularity of the mesh $\mathcal{T}_h$. ∎

4.2. **Gauss-compatibility of the non-conforming Maxwell solver**

We now establish that the above scheme can be made Gauss-compatible and give a priori error estimates leading to long-time stability. Again we denote $U_h = (cB_h, \boldsymbol{E}_h)^T$ and $F = (0, \varepsilon_0^{-1}\boldsymbol{J})^T$. In compact form, the non-conforming Conga-Ampère scheme (4.2) reads $\partial_t U_h - \mathcal{A}_h U_h = -F_h = -\Pi_h F$ with a composite curl operator that takes a form similar to (3.20) but involves additional projection operators. Specifically, it is defined on $\mathcal{V}_h := \tilde{V}_h^1 \times V_h^2$ by

$$\mathcal{A}_h := c\begin{pmatrix} 0 & -\operatorname{curl}_h \\ \mathbf{curl}_h & 0 \end{pmatrix} \qquad \text{with} \qquad \begin{cases} \mathbf{curl}_h := \mathbf{curl}\,\mathcal{P}_h^1|_{\tilde{V}_h^1} : \tilde{V}_h^1 \to V_h^2 \\ \operatorname{curl}_h := (\mathbf{curl}_h)^* : V_h^2 \to \tilde{V}_h^1. \end{cases} \tag{4.11}$$

According to Definition 2.3 and using approximation projection operators of the form (3.21), we then see that this scheme is Gauss-compatible on some product space $\hat{V}^1 \times \hat{V}^2$ if for $l = 1, 2$ we can find approximation operators π_h^l and $\hat{\pi}_h^l$ mapping on V_h^l, such that

$$\pi_h^2\,\mathbf{curl}\,u = \mathbf{curl}\,\mathcal{P}_h^1\hat{\pi}_h^1 u, \qquad u \in \hat{V}^1 \tag{4.12}$$

and

$$\pi_h^1 \operatorname{curl} \boldsymbol{u} = (\mathbf{curl}_h)^*\hat{\pi}_h^2\boldsymbol{u}, \qquad \boldsymbol{u} \in \hat{V}^2. \tag{4.13}$$

The following compatibility result is then easy to verify.

Theorem 4.3. *The Conga-Ampère scheme* (4.2) *associated with the Raviart-Thomas interpolation* (3.15) *for the current, $\pi_h^2 := \pi_h^{\rm div}$, is Gauss-compatible on the product space*

$$\hat{V}^1 \times \hat{V}^2 := \mathcal{C}(\Omega) \times \boldsymbol{H}_0(\operatorname{curl};\Omega).$$

Specifically, Equation (4.12) *holds with the operator* $\hat{\pi}_h^1 := \pi_h^{\mathbf{curl}}$ *defined in* (3.10)*, and Equation* (4.13) *holds on* $\boldsymbol{H}_0(\mathrm{curl};\Omega)$ *with* $\pi_h^1 := (\mathcal{P}_h^1)^*$ *and* $\hat{\pi}_h^2 := P_{V_h^2}$*. Moreover, these mappings satisfy*

$$\|\hat{\pi}_h^1 u - u\| \lesssim h^m |u|_m, \qquad 2 \le m \le p+1 \tag{4.14}$$

$$\|\hat{\pi}_h^2 \boldsymbol{u} - \boldsymbol{u}\| \lesssim h^m |\boldsymbol{u}|_m, \qquad 0 \le m \le p \tag{4.15}$$

$$\|\pi_h^1 u - u\| \lesssim h^m |u|_m, \qquad 0 \le m \le \max(1, p-2) \tag{4.16}$$

$$\|\pi_h^2 \boldsymbol{u} - \boldsymbol{u}\| \lesssim h^m |\boldsymbol{u}|_m, \qquad 1 \le m \le p. \tag{4.17}$$

Proof. Equation (4.12) is obtained by applying again the standard commuting diagram recalled in Lemma 3.4 and using the fact that $\mathcal{P}_h^1 = I$ on V_h^1. To show next that (4.13) holds as stated, i.e.,

$$(\mathcal{P}_h^1)^* \operatorname{curl} \boldsymbol{u} = (\mathbf{curl}_h)^* P_{V_h^2} \boldsymbol{u}, \qquad \boldsymbol{u} \in V_2^* = \boldsymbol{H}_0(\mathrm{curl};\Omega), \tag{4.18}$$

we observe that both sides belong to $\tilde{V}_h^1$ by construction, so that we can test this equality against an arbitrary $v \in \tilde{V}_h^1$ and use the definition of the various operators to compute

$$\langle (\mathcal{P}_h^1)^* \operatorname{curl} \boldsymbol{u}, v\rangle = \langle \operatorname{curl} \boldsymbol{u}, \mathcal{P}_h^1 v\rangle = \langle \boldsymbol{u}, \mathbf{curl}\, \mathcal{P}_h^1 v\rangle = \langle P_{V_h^2}\boldsymbol{u}, \mathbf{curl}\, \mathcal{P}_h^1 v\rangle = \langle (\mathbf{curl}_h)^* P_{V_h^2}\boldsymbol{u}, v\rangle$$

which proves (4.18). Estimates (4.14), (4.15), (4.16) and (4.17) are then just (3.24), (3.25), (4.10) and (3.16) respectively. ∎

If one is solving the Maxwell equations with exact sources, Theorem 2.5 applies and gives the following a priori estimate.

Corollary 4.4. *Let* $(B, \boldsymbol{E})$ *be the exact solution to the Maxwell system* (2.22)*. The semi-discrete solution to the non-conforming Conga-Ampère scheme* (4.2) *coupled with the Raviart-Thomas interpolation* (3.15) *for the current satisfies*

$$\begin{aligned}\|(B - B_h)(t)\| + \|(\boldsymbol{E} - \boldsymbol{E}_h)(t)\| &\lesssim \|B_h(0) - \hat{\pi}_h^1 B(0)\| + \|\boldsymbol{E}_h(0) - \hat{\pi}_h^2 \boldsymbol{E}(0)\| \\ &+ h^{\hat{m}}\Big(|B(0)|_{\hat{m}} + \int_0^t |\partial_t B(s)|_{\hat{m}}\,\mathrm{d}s\Big) + h^m \int_0^t |\partial_t B(s)|_m\,\mathrm{d}s + h^{m'}\Big(|\boldsymbol{E}(0)|_{m'} + \int_0^t |\partial_t \boldsymbol{E}(s)|_{m'}\,\mathrm{d}s\Big)\end{aligned}$$

for $2 \le \hat{m} \le p+1$*,* $0 \le m \le \max(1, p-2)$*,* $1 \le m' \le p$ *and with a constant independent of* h *and* t*.*

Remark 4.5. In the case of approximate sources, one must resort to the analysis developped in Section 2.4 to be able to derive long-time stability estimates. This will be done in Section 5.2 by showing that the Conga-Ampère scheme (3.6) can be equipped with a non-standard divergence that makes it structure-preserving.

5. Application to coupled problems

In this section we apply the new stability analysis proposed in Section 2.1 and 2.4 for approximate sources: in Section 5.1 we begin by verifying that the conforming Finite Element discretization studied in Section 3 is naturally structure-preserving in the sense of Definition 2.11, and in Section 5.2 we show that our new non-conforming Conga discretization of Section 4 is also structure-preserving, once associated with a nonstandard discrete divergence. Assuming next a discrete particle representation of the approximate current density, we provide a current deposition method that makes both Maxwell schemes charge-conserving in the sense of Definition 2.16.

To specify the problem we consider the case where the Maxwell system is coupled with a Vlasov equation such as (1.1) involving a species of charged particles with phase space distribution function

$f = f(t, \boldsymbol{x}, \boldsymbol{v})$. The charge and current densities are then given by the first moments of f,

$$\rho(t, \boldsymbol{x}) := q \int f(t, \boldsymbol{x}, \boldsymbol{v}) \, \mathrm{d}\boldsymbol{v} \qquad \text{and} \qquad \boldsymbol{J}(t, \boldsymbol{x}) := q \int \boldsymbol{v} f(t, \boldsymbol{x}, \boldsymbol{v}) \, \mathrm{d}\boldsymbol{v}. \tag{5.1}$$

5.1. **Structure-preserving discretization with conforming Finite Elements**

The structure-preserving properties of the conforming Maxwell scheme (3.6) essentially follow from the fact that $\mathbb{R} \xrightarrow{\iota} V_h^1 \xrightarrow{\mathbf{curl}} V_h^2 \xrightarrow{\mathrm{div}} V_h^3$ is an exact sequence, as recalled in Lemma 3.2. The Poincaré estimates (2.40) are also standard to verify. Since ι_h is just the canonical injection ι the first estimate is trivial. The second one

$$\|u\| \leq c_P \|\mathbf{curl}\, u\|, \quad u \in V_h^1 \cap (\ker \mathbf{curl})^\perp \tag{5.2}$$

is just the Poincaré-Wirtinger inequality (indeed in 2D we have $\|\mathbf{curl}\, u\| = \|\mathbf{grad}\, u\|$ and $(\ker \mathbf{curl})^\perp$ contains only zero-average functions). As for the third one

$$\|\boldsymbol{u}\| \leq c_P \|\mathrm{div}\, \boldsymbol{u}\|, \quad \boldsymbol{u} \in V_h^2 \cap (\ker \mathrm{div})^\perp \tag{5.3}$$

it can be derived from the classical stability estimates established for the Raviart-Thomas elements (use for instance [63, Th. 4] which states that for each $v \in V_h^3$ there exists $\boldsymbol{w} \in V_h^2$ such that $\mathrm{div}\, \boldsymbol{w} = v$ and $\|\boldsymbol{w}\| \leq C\|v\|$ with a constant independent of h, and observe that $\boldsymbol{u}$ in $(\ker \mathrm{div})^\perp$ has the smallest L^2 norm among all the $\boldsymbol{w} \in V_h^2$ such that $\mathrm{div}\, \boldsymbol{w} = \mathrm{div}\, \boldsymbol{u}$). Hence we have the following Lemma.

Lemma 5.1. *The conforming scheme* (3.6) *associated with the discrete Gauss laws* (2.38) *defined by*

$$\begin{cases} \iota_h = \iota : \mathbb{R} \to V_h^1 \\ \mathrm{div}_h = \mathrm{div}\,|_{V_h^2} : V_h^2 \to V_h^3 \end{cases} \tag{5.4}$$

see (3.2)-(3.5)*, is structure preserving in the sense of Definition 2.11.*

5.2. **Structure-preserving discretization with the discontinuous Conga method**

In order to study the structure-preserving properties of the Conga method, and identify the proper discrete divergence operators, we first characterize the kernel and the image of the non-conforming curl operator following the method introduced in [15].

Lemma 5.2. *The non-conforming curl operator* (4.11), $\mathbf{curl}_h := \mathbf{curl}\, \mathcal{P}_h^1|_{\tilde{V}_h^1} : \tilde{V}_h^1 \mapsto V_h^2$, *satisfies*

$$\ker(\mathbf{curl}_h) = \mathbb{R} \oplus (I - \mathcal{P}_h^1)\tilde{V}_h^1 \qquad \textit{and} \qquad \mathrm{Im}(\mathbf{curl}_h) = \ker \mathrm{div}_h \, .$$

Proof. Starting with the first identity, the inclusion $\supset$ is easily verified by applying $\mathbf{curl}\, \mathcal{P}_h^1$. To verify the inclusion $\subset$ we take $u \in \ker(\mathbf{curl}_h) = \tilde{V}_h^1 \cap \ker(\mathbf{curl}\, \mathcal{P}_h^1)$. Then $\mathcal{P}_h^1 u$ is in $V_h^1 \cap \ker \mathbf{curl}$ which coincides with $\mathbb{R}$. Hence we have

$$u = \mathcal{P}_h^1 u + (I - \mathcal{P}_h^1)u \in \mathbb{R} \oplus (I - \mathcal{P}_h^1)\tilde{V}_h^1,$$

and we note that this is an orthogonal sum since $(\mathcal{P}_h^1)^*$ preserves the constants, see Lemma 4.2. The second identity follows from Lemma 3.2 and the fact that $\mathcal{P}_h^1 \tilde{V}_h^1 = V_h^1$. ∎

We are then in position to establish that the Conga-Ampère scheme is structure preserving when associated with the proper discrete operators for the Gauss laws.

Lemma 5.3. *The non-conforming Conga scheme* (4.2) *associated with the discrete Gauss laws* (2.38) *defined by*

$$\begin{cases} \iota_h : (\mathbb{R} \times \tilde{V}_h^1) \ni (a, \tilde{u}) \mapsto a + (I - \mathcal{P}_h^1)\tilde{u} \in \tilde{V}_h^1 \\ \mathrm{div}_h = \mathrm{div}\,|_{V_h^2} : V_h^2 \to V_h^3 \end{cases} \tag{5.5}$$

see (3.2)-(3.5)*, is structure preserving in the sense of Definition 2.11.*

Remark 5.4. With the proposed operator ι_h, the discrete Gauss laws (2.38) read

$$\begin{cases} \mathrm{div}\, \boldsymbol{E}_h(t) = \dfrac{1}{\varepsilon_0}\rho_h(t) & \text{in } V_h^3 \\ \langle B_h(t), a + (I - \mathcal{P}_h^1)\tilde{u}\rangle = \langle B_h^0, a + (I - \mathcal{P}_h^1)\tilde{u}\rangle & \text{for } (a, \tilde{u}) \in \mathbb{R} \times \tilde{V}_h^1. \end{cases}$$

Proof. Here the exact sequence property (2.39), namely

$$\mathbb{R} \times \tilde{V}_h^1 \xrightarrow{\ \iota_h\ } \tilde{V}_h^1 \xrightarrow{\ \mathbf{curl}_h = \mathbf{curl}\,\mathcal{P}_h^1\ } V_h^2 \xrightarrow{\ \mathrm{div}\ } V_h^3 \tag{5.6}$$

with ι_h defined in (5.5), follows from Lemma 5.2. To prove the stability estimates in (2.40) we follow the proof of Theorem 4.1 from [16].
We begin by observing that

$$\ker \iota_h = \{0\} \times V_h^1,$$

indeed $(a, \tilde{u}) \in \ker \iota_h$ satisfies $(I - \mathcal{P}_h^1)\tilde{u} \in \mathbb{R} \subset V_h^1$, hence $\tilde{u} \in V_h^1$ and $a = 0$, and the converse inclusion is straightforward. Considering then $\tilde{u} \in \tilde{V}_h^1 \cap (V_h^1)^\perp$, we write

$$\begin{aligned} \|(a, \tilde{u})\|^2 := |\Omega||a|^2 + \|\tilde{u}\|^2 &\le 2\|a - \mathcal{P}_h^1\tilde{u}\|^2 + 2\|\mathcal{P}_h^1\tilde{u}\|^2 + \|\tilde{u}\|^2 \\ &\le 2(\|\mathcal{P}_h^1\|^2 + 1)(\|a - \mathcal{P}_h^1\tilde{u}\|^2 + \|\tilde{u}\|^2) = 2(\|\mathcal{P}_h^1\|^2 + 1)\|a + (I - \mathcal{P}_h^1)\tilde{u}\|^2 \end{aligned}$$

where the last equality uses that $a - \mathcal{P}_h^1\tilde{u}$ is in V_h^1 and hence is orthogonal to $\tilde{u}$. Thus we have

$$\|(a, \tilde{u})\| \le (2(\|\mathcal{P}_h^1\|^2 + 1))^{\frac{1}{2}}\|\iota_h(a, \tilde{u})\|, \qquad (a, \tilde{u}) \in (\mathbb{R} \times \tilde{V}_h^1) \cap (\ker \iota_h)^\perp,$$

which is the first stability estimate in (2.40). For the second estimate we use again the identity $\ker \mathbf{curl}_h = \mathbb{R} \oplus (I - \mathcal{P}_h^1)\tilde{V}_h^1$ and consider now

$$\tilde{u} \in \tilde{V}_h^1 \cap (\ker \mathbf{curl}_h)^\perp = \tilde{V}_h^1 \cap \mathbb{R}^\perp \cap ((I - \mathcal{P}_h^1)\tilde{V}_h^1)^\perp$$

and let $u \in V_h^1 \cap (\ker \mathbf{curl})^\perp = V_h^1 \cap \mathbb{R}^\perp$ be defined by $\mathbf{curl}\, u = \mathbf{curl}\, \mathcal{P}_h^1\tilde{u}$. This implies that the difference $u - \mathcal{P}_h^1\tilde{u}$ is in $\ker \mathbf{curl} = \mathbb{R}$, hence it is orthogonal to $\tilde{u}$. Because the latter is also orthogonal to $(I - \mathcal{P}_h^1)\tilde{u}$, we find that it is orthogonal to $\tilde{u} - u$. Using this and the conforming Poincaré estimate (5.2) for u we compute

$$\|\tilde{u}\| \le (\|\tilde{u}\|^2 + \|u - \tilde{u}\|^2)^{\frac{1}{2}} = \|u\| \le c_P\|\mathbf{curl}\, u\| = c_P\|\mathbf{curl}\, \mathcal{P}_h^1\tilde{u}\|$$

which proves the second stability estimate in (2.40) for the non-conforming sequence (5.6). Finally the third estimate is just (5.3) as in the conforming case, and the proof is complete. ∎

5.3. **Charge-conserving coupling with smooth particles**

In the particle method the phase-space distribution function f solution to (1.1) is approached by a sum of N (macro) particles with positions $\boldsymbol{x}_\kappa(t)$ and velocities $\boldsymbol{v}_\kappa(t) = \boldsymbol{x}_\kappa'(t)$, $\kappa = 1, \dots N$, that are pushed forward along the integral curves of the semi-discrete force field computed by the Maxwell scheme, using some given ODE solver. The approximated density is then

$$f_N(t, \boldsymbol{x}, \boldsymbol{v}) = \sum_{\kappa=1}^{N} q_\kappa \zeta_\varepsilon(\boldsymbol{x} - \boldsymbol{x}_\kappa(t))\zeta_\varepsilon(\boldsymbol{v} - \boldsymbol{v}_\kappa(t)) \tag{5.7}$$

where q_κ is the numerical charge associated with the κ-th (macro) particle and ζ_ε is a shape function supported in the Ball $B(0,\varepsilon)$ of center 0 and radius $\varepsilon \geq 0$, which can either be a smooth approximation of the Dirac measure if $\varepsilon > 0$ (typically a spline with unit mass, see e.g. [43]) or the Dirac measure itself if $\varepsilon = 0$. The corresponding approximations for the charge and current densities read then

$$\rho_N(t,\boldsymbol{x}) := \sum_{\kappa=1}^{N} q_\kappa \zeta_\varepsilon(\boldsymbol{x} - \boldsymbol{x}_\kappa(t)) \qquad \text{and} \qquad \boldsymbol{J}_N(t,\boldsymbol{x}) := \sum_{\kappa=1}^{N} q_\kappa \boldsymbol{v}_\kappa(t) \zeta_\varepsilon(\boldsymbol{x} - \boldsymbol{x}_\kappa(t)). \tag{5.8}$$

We observe that since $\boldsymbol{v}_\kappa(t) = \boldsymbol{x}'_\kappa(t)$, these particle densities satisfy an exact continuity equation,

$$\operatorname{div} \boldsymbol{J}_N = \sum_{\kappa=1}^{N} q_\kappa \operatorname{div}\left(\boldsymbol{v}_\kappa \zeta_\varepsilon(\cdot - \boldsymbol{x}_\kappa)\right) = \sum_{\kappa=1}^{N} q_\kappa \boldsymbol{v}_\kappa \cdot \mathbf{grad}\, \zeta_\varepsilon(\cdot - \boldsymbol{x}_\kappa) = -\sum_{\kappa=1}^{N} q_\kappa \partial_t \zeta_\varepsilon(\cdot - \boldsymbol{x}_\kappa) = -\partial_t \rho_N. \tag{5.9}$$

In the case where $\varepsilon = 0$ we note that the above equalities hold in the sense of distributions. In this paper we restrict ourselves to the case of smooth particles ($\varepsilon > 0$) and leave the case of Dirac particles for a future study, see Remark 3.9.

In order to make both the conforming and non-conforming schemes charge-conserving in the sense of Definition 2.16 we must then find a proper approximation $\boldsymbol{J}_h$ for the particle current $\boldsymbol{J}_N$. The following result shows that for this task we can use the Raviart-Thomas interpolation, just as for the compatibility results stated in Sections 3.4 and 4.2.

Theorem 5.5. *The respective conforming (FEM) and non-conforming (Conga) schemes* (3.6) *and* (4.2)*, associated with the discrete Gauss laws* (2.38) *defined by the discrete divergence operators* (5.4) *and* (5.5) *respectively, are charge-conserving in the sense of Definition 2.16 when the discrete sources are defined from the particle charge and current densities* (5.8) *by*

$$\rho_h(t) := P_{V_h^3} \rho_N(t) \in V_h^3 \qquad \text{and} \qquad \boldsymbol{J}_h(t) := \pi_h^{\mathrm{div}} \boldsymbol{J}_N(t) \in V_h^2 \tag{5.10}$$

where $P_{V_h^3}$ is the L^2 (orthogonal) projection on the discontinuous space V_h^3 and π_h^{div} is the canonical Raviart-Thomas interpolation recalled in Section 3.3.

Proof. Since we already know that (3.6) and (4.2) are structure preserving when associated with the respective divergence operators (5.4) and (5.5), it suffices to note that in both cases the proper discrete divergence is just the restriction of the exact div to the Raviart-Thomas space V_h^2, and to observe that

$$\operatorname{div} \boldsymbol{J}_h = \operatorname{div} \pi_h^{\mathrm{div}} \boldsymbol{J}_N = P_{V_h^3} \operatorname{div} \boldsymbol{J}_N = -P_{V_h^3} \partial_t \rho_N = -\partial_t \rho_h$$

follows from the commuting diagram (3.17) and the continuity equation (5.9) satisfied by the particle sources. ∎

6. Numerical results

In this section we illustrate the proposed FEM and Conga methods on a couple of simple but relevant test cases. For this purpose we use an explicit leap-frog time discretization of the form

$$\begin{cases} \dfrac{1}{\Delta t}(B_h^{n+1/2} - B_h^{n-1/2}) + \operatorname{curl}_h \boldsymbol{E}_h^n = 0 \\ \dfrac{1}{\Delta t}(\boldsymbol{E}_h^{n+1} - \boldsymbol{E}_h^n) - c^2\, \mathbf{curl}_h\, B_h^{n+1/2} = -\dfrac{1}{\varepsilon_0} \boldsymbol{J}_h^{n+1/2} \end{cases} \tag{6.1}$$

in addition to the FEM or Conga discretization in space, defined in (3.6) and (4.2) respectively.

Remark 6.1. When studying the Conga method we have observed that the smoothed field $\mathcal{P}_h^1 B_h$ was more accurate than the discontinuous field B_h itself: for the studied cases, it had smaller errors and higher convergence rates. Therefore we have decided to use the smoothed projection $\mathcal{P}_h^1$ as a systematic post-processing filter. We remind that this is a local operation on the discrete fields, hence its effect on the overall computational time is not significant.

6.1. **A Pure Maxwell problem: the 2D Issautier test case**

To assess the basic convergence and stability properties of the proposed schemes we use the analytical current source proposed in [42, 29] to study the charge conservation properties of a penalized finite volume scheme, and also considered in [68] to assess the stability of DG solvers with hyperbolic field correction. The problem is posed in a metallic cavity $\Omega = [0,1]^2$ with articifial permittivity ε_0 and light speed c equal to one, and the current density is given as

$$\boldsymbol{J}(t,x,y) = (\cos(t)-1)\begin{pmatrix}\pi\cos(\pi x)+\pi^2 x\sin(\pi y)\\ \pi\cos(\pi y)+\pi^2 y\sin(\pi x)\end{pmatrix} - \cos(t)\begin{pmatrix}x\sin(\pi y)\\ y\sin(\pi x)\end{pmatrix}. \tag{6.2}$$

We consider initial fields $\boldsymbol{E}^0 = 0$ and $B^0 = 0$, so that the exact solution is

$$\begin{cases}\boldsymbol{E}(t,x,y) = \sin(t)\begin{pmatrix}x\sin(\pi y)\\ y\sin(\pi x)\end{pmatrix}\\ B(t,x,y) = (\cos(t)-1)\big(\pi y\cos(\pi x) - \pi x\cos(\pi y)\big).\end{cases} \tag{6.3}$$

We note that the associated charge density reads then $\rho(t,x,y) = \sin(t)\big(\sin(\pi x)+\sin(\pi y)\big)$.

In Figure 6.1 we first assess the convergence properties of the two proposed methods by plotting the relative L^2 errors $e_h := \max\left(\|\boldsymbol{E}-\boldsymbol{E}_h\|/\|\boldsymbol{E}\|, \|B-B_h\|/\|B\|\right)$ at time $t = 0.2\pi$. In the left plot we show the results obtained with the conforming FEM (3.6) using different degrees and in the right plot we show the errors corresponding to the non-conforming Conga method (4.2). We observe that the FEM solutions converge at the expected rates, see Corollary 3.6. The good news is that the Conga solutions converge at a rate close to $\max(1, p-1)$ which is about one order better than the one announced in Corollary 4.4. In particular, we have observed that the accuracy of both first order methods was very comparable, and for $p > 1$ the accuracy of the Conga solutions (smoothed as described in Remark 6.1) of degree $p+1$ was very similar, if not better, to that of the conforming solutions of degree p.

Time wise, we have observed that with our straightforward implementation the Conga simulations were more efficient than the FEM ones when the meshes became finer, which is not surprising since the former is purely local and does not require any global matrix inversion. Specifically, our simulations have shown that for $p > 1$, the computational time of the FEM method with degree p becomes higher than that of the Conga method with degree $p+1$, as soon as the mesh has more than about 6000 triangles (which corresponds to $h \leq 0.06$ for the meshes used here).

In order to assess the long-time properties of the solutions computed when the discrete current density is obtained with the Raviart-Thomas interpolation operator

$$\boldsymbol{J}_h^{n+\frac{1}{2}} = \pi_h^{\mathrm{div}} \boldsymbol{J}(t^{n+\frac{1}{2}}) \tag{6.4}$$

as supported by our analysis, we have plotted in the left panel of Figure 6.2 the L^2 norm of the solutions computed with the FEM method (3.6) of degree $p = 2$, using a mesh with about 250 triangles ($h \approx 0.3$). For comparison we have plotted on the right panel the norm of the solutions obtained similarly, but using a naive L^2 projection on the Raviart-Thomas space for the current density, i.e.,

$$\boldsymbol{J}_h^{n+\frac{1}{2}} = P_{V_h^2} \boldsymbol{J}(t^{n+\frac{1}{2}}). \tag{6.5}$$

In the latter case a rapid (linear in time) deterioration of the solution is visible, but with the Gauss-compatible scheme the solution is stable, as predicted by Corollaries 2.6 and 2.7, applied to the constant

and time-harmonic parts of the Issautier field (6.3). Note that here we have only shown the curves of the electric field, as those of the magnetic field were always on top of the reference curves (dashed) computed from the exact solutions. We have also decided not to show the curves obtained with the non-conforming Conga method, as they were very similar to those in Figure 6.2.

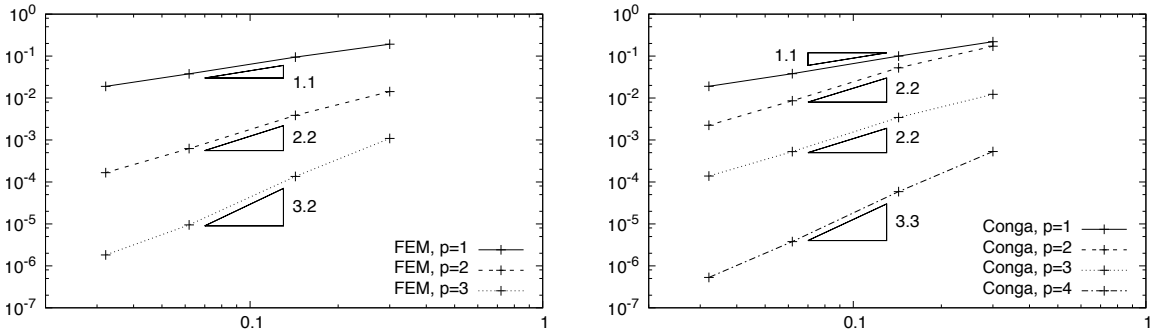

FIGURE 6.1. Convergence curves (relative errors vs. maximal triangle diameter h) for the Issautier problem with analytical source (6.2). Results obtained with the conforming FEM discretization are shown left, and those obtained with the non-conforming Conga discretization are shown right.

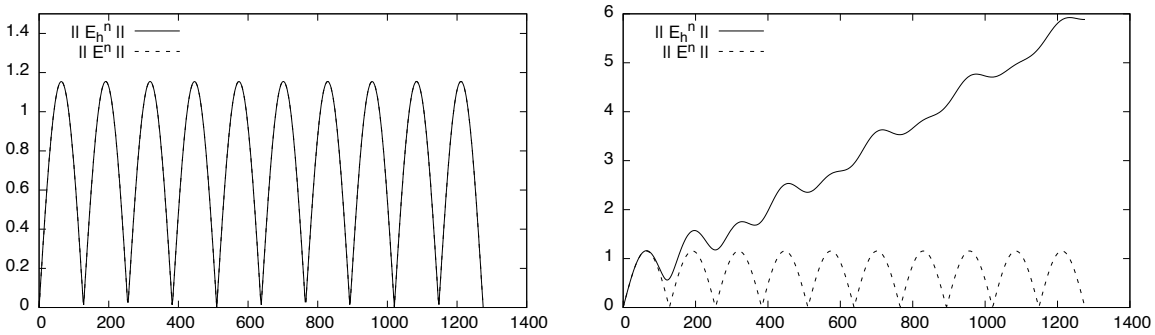

FIGURE 6.2. Evolution of the L^2 norm of the electric field for the Issautier problem. On the left plot the numerical solution is obtained by approximating the current density with the Raviart-Thomas interpolation (6.4), whereas on the right plot the current density is approximated using a standard L^2 projection on the $\boldsymbol{H}(\mathrm{div})$-conforming Raviart-Thomas space V_h^2, see (6.5). For comparison, the norm of the exact solution is shown in dashed lines (on the left plot it is on top of the solid line).

6.2. **A Vlasov-Maxwell problem: an academic diode test case**

Electromagnetic PIC schemes are a popular approach to model the propagation of charged particle beams in vacuum devices, see for instance [44, 67, 26] demonstrating the numerical efficiency of DG-PIC schemes using divergence cleaning techniques, or [60] where a conforming FEM scheme using low order Nédélec elements (Whitney forms) is coupled with particles using a charge-conserving deposition method.

To assess the accuracy and stability properties of the charge-conserving FEM-PIC and Conga-PIC methods proposed in this article, we will use the academic diode test case described in [18].

Although more advanced Vlasov-Maxwell test cases have been used in [69, 19] to show some benefits of charge-conserving deposition schemes over divergence cleaning techniques, we note that simple diodes are a standard test-case to validate the basic properties of charge-conserving particle methods, see e.g. [5, 17, 66].

Here the domain is a square $\Omega = [0, 0.1\text{m}]^2$ with metallic boundary $\Gamma_M = \{0, 0.1\text{m}\} \times [0, 0.1\text{m}]$ and absorbing boundary $\Gamma_A =]0, 0.1\text{m}[\times\{0, 0.1\text{m}\}$. On the left boundary a beam of electrons is steadily injected and accelerated by a constant external field which derives from the electric potential imposed on both the cathode ($\phi_{\text{ext}} = 0$ on the left boundary) and the anode ($\phi_{\text{ext}} = 10^5\text{V}$ on the right boundary). Due to the propagation of the beam into the domain (initially empty of charges) a self-consistent electro-magnetic field develops and is added to this constant external field, and in turn the trajectories of the electrons are no longer straight lines. However this modification is of small relative amplitude and the resulting solution tends towards a smooth steady state, so that the convergence of the numerical approximations can be easily assessed. In Figure 6.3 we show the typical profile of the solution in the steady state regime (self-consistent electric field on the left and particles on the right), together with the mesh used in the simulations.

To deposit the current carried by the smooth particles we have implemented an approximated version of the Raviart-Thomas interpolation operator π_h^{div} using Fekete quadrature formulas. In addition to having good interpolation properties, the Fekete points on a triangle have the convenient property to contain the quadrature (Gauss-Lobatto) points on the edges, as a subset. It is then possible to reuse the (quite expensive) current contributions computed on these points when computing the edge-based degrees of freedom of the deposited current. For the smooth particles we have used second-order shapes proposed by Jacobs and Hesthaven in [43]. These shapes have the advantage of being polynomial on their support unlike spline particles which are made of several polynomial pieces. Because the long-term charge conservation properties of the scheme require an accurate time-average of the particle current in the deposition method as demonstrated in [30, 17], this feature actually simplifies the involved algorithms. For more details on these algorithms we refer to [18].

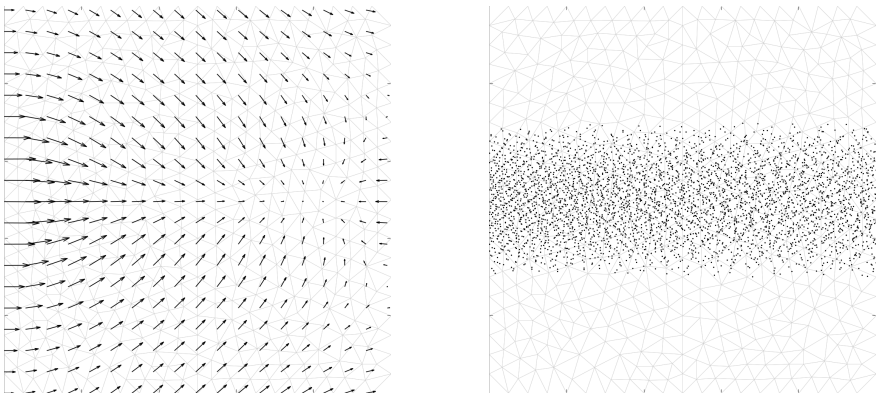

Figure 6.3. Academic beam test case. The self-consistent $\boldsymbol{E}$ field (left plot) and the numerical particles accelerated towards the right boundary (right plot) show the typical profile of the solution in the steady state regime. For the considered geometry the external field is constant $\boldsymbol{E}_{\text{ext}} = (-10^6, 0)\text{Vm}^{-1}$.

To assess the numerical stability properties of the proposed FEM and Conga methods over long time ranges we plot in Figure 6.4 the profiles of some fields computed with the Conga-PIC scheme, using a final time chosen such that the particles have travelled approximatively five diode lengths.

On the left panels the fields have been computed by coupling the Conga scheme (4.2) with the charge-conserving deposition (5.10). For comparison, we have shown the solutions obtained by coupling the

same Conga scheme with a standard L^2 deposition (projection) of the smooth particle current on the Raviart-Thomas space V_h^2. Because this L^2 projection does not satisfy a commuting diagram similar to (3.17), the resulting coupled scheme is a priori not charge-conserving, and as expected the simulations exhibit a deterioration of the electric field that grows linearly in time and is clearly visible in the left panels of Figure 6.4. The very good stability of the solution computed with the charge-conserving deposition (5.10) is a strong indication that our analysis has produced a better scheme.

As for the conforming FEM method (coupled either with a standard L^2 projection or with the charge-conserving deposition (5.10)), very similar results have been obtained which are not shown here, leading to a similar conclusion.

7. Conclusion

In this series of papers we have provided a rigorous solution to the longstanding problem of charge-conserving coupling between general Maxwell solvers and particle methods, following the classical approach developped by plasma physicists over the last decades. Our stability analysis extends a recent work on compatible source approximation operators for pure Maxwell solvers, and it is based on the notion of discrete de Rham structure. This abstract setting allows us to design charge-conserving deposition schemes for general conforming but also non-conforming Maxwell discretizations, thus offering an interesting alternative to divergence cleaning methods to stabilize discontinuous Galerkin Particle-in-Cell solvers.

The framework of de Rham sequences also allows the choice of discretizing either the Ampère or the Faraday equation strongly, the other being handled by duality. In this paper we provided the discrete framework for a strong Ampère equation and verified that it can be applied to a classical conforming Finite Element discretization, and also to a new hybrid non-conforming discretization having the advantage of avoiding global coupling.

Numerical experiments using a pure Maxwell problem and a simple diode configuration allowed us to validate the theoretical stability of the proposed methods. Future studies should now address more elaborate test-cases to better understand the benefits of these structure-preserving and charge-conserving solvers with a strong Ampère law. Another open problem of interest is the one of extending the proposed deposition schemes for low-regularity current densities.

Acknowledgements

The authors would like to thank Stéphanie Salmon, Marie Mounier and Mathieu Lutz for stimulating discussions. They also acknowledge the anonymous referees for the questions and comments that helped clarify the presentation of this work.

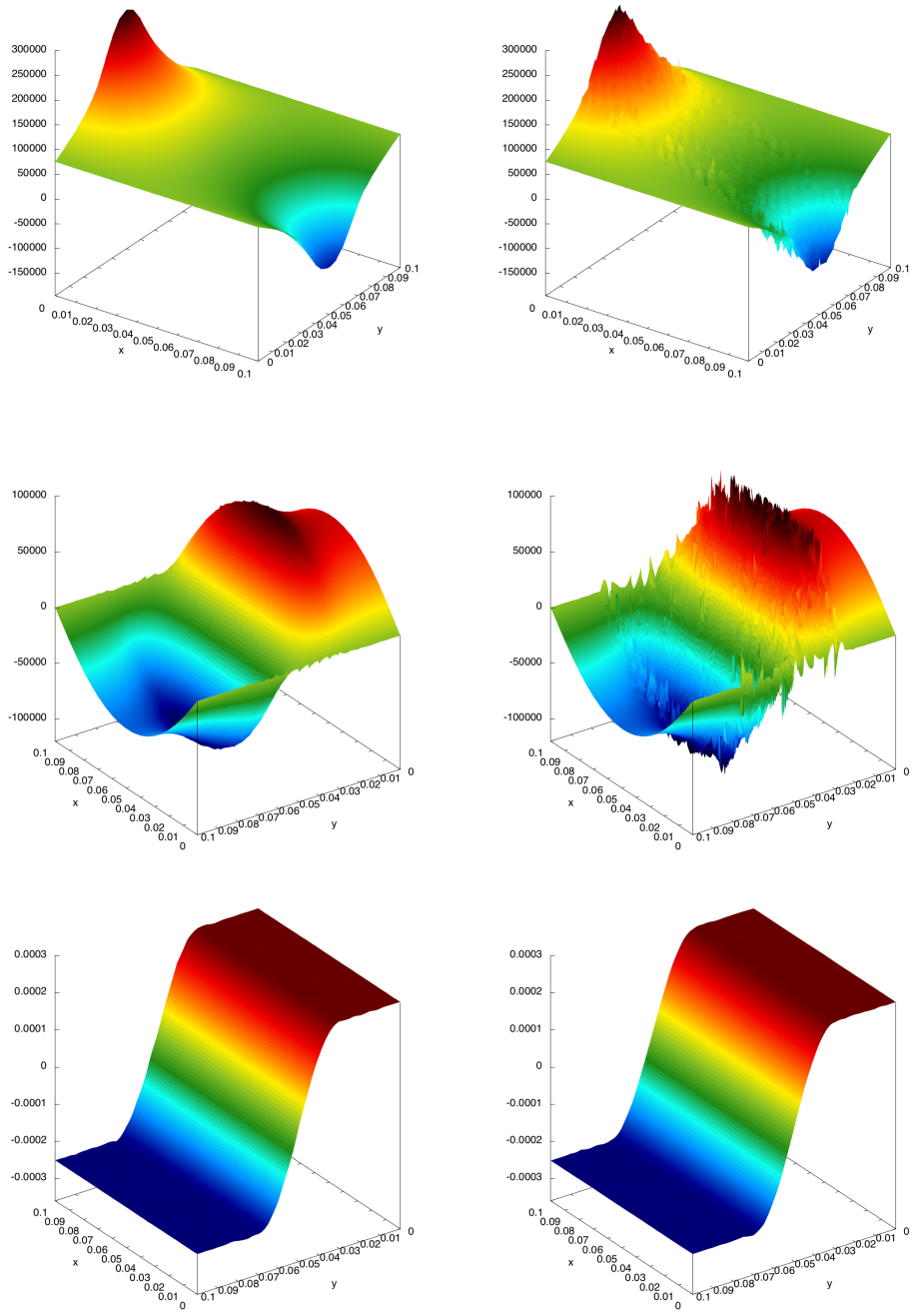

Figure 6.4. Academic beam test-case. Snapshots of the self-consistent fields (E_x on the top row, E_y on the center row and B on the bottom row) obtained by deposing the conservative current density carried by the particles either with the charge-conserving scheme implementing the Raviart-Thomas interpolation operator π_h^{div} on V_h^2 (left plots) or with an L^2 projection on the div-conforming space V_h^2 (right plots). In both cases the scheme is a non-conforming Conga scheme (4.2) with degree $p = 2$, using a mesh of approximately 1000 triangles and 10 smooth particles per cell.

References

[1] J.-C. Adam, A. Gourdin Serveniere, J.-C. Nédélec, and P.-A. Raviart. Study of an implicit scheme for integrating Maxwell's equations. *Computer Methods in Applied Mechanics and Engineering*, 22:327–346, 1980.

[2] D.N. Arnold, R.S. Falk, and R. Winther. Finite element exterior calculus, homological techniques, and applications. *Acta Numerica*, 2006.

[3] D.N. Arnold, R.S. Falk, and R. Winther. Geometric decompositions and local bases for spaces of finite element differential forms. *Computer Methods in Applied Mechanics and Engineering*, 198(21):1660–1672, 2009.

[4] D.N. Arnold, R.S. Falk, and R. Winther. Finite element exterior calculus: from Hodge theory to numerical stability. *Bull. Amer. Math. Soc.(NS)*, 47(2):281–354, 2010.

[5] R. Barthelmé and C. Parzani. Numerical charge conservation in particle-in-cell codes. In *Numerical methods for hyperbolic and kinetic problems*, pages 7–28. Eur. Math. Soc., Zürich, 2005.

[6] D. Boffi. A note on the deRham complex and a discrete compactness property. *Applied Mathematics Letters*, 14(1):33–38, January 2001.

[7] D. Boffi. Compatible Discretizations for Eigenvalue Problems. In *Compatible Spatial Discretizations*, pages 121–142. Springer New York, New York, NY, 2006.

[8] D. Boffi, F. Brezzi, and M. Fortin. *Mixed finite element methods and applications*, volume 44 of *Springer Series in Computational Mathematics*. Springer, 2013.

[9] J.P. Boris. Relativistic plasma simulations - optimization of a hybrid code. In *Proc. 4th Conf. Num. Sim. of Plasmas, (NRL Washington, Washington DC)*, pages 3–67, 1970.

[10] A. Bossavit. Whitney forms: a class of finite elements for three-dimensional computations in electromagnetism. In *Physical Science, Measurement and Instrumentation, Management and Education - Reviews, IEE Proceedings A*, pages 493–500, 1988.

[11] A. Bossavit. *Computational electromagnetism: variational formulations, complementarity, edge elements*. Academic Press, 1998.

[12] H. Brezis. *Functional analysis, Sobolev spaces and partial differential equations*. Springer, 2010.

[13] A. Buffa and I. Perugia. Discontinuous Galerkin Approximation of the Maxwell Eigenproblem. *SIAM Journal on Numerical Analysis*, 44(5):2198–2226, January 2006.

[14] A. Buffa, G. Sangalli, and R. Vázquez. Isogeometric analysis in electromagnetics: B-splines approximation. *Computer Methods in Applied Mechanics and Engineering*, 199(17):1143–1152, 2010.

[15] M. Campos Pinto. Constructing exact sequences on non-conforming discrete spaces. *Comptes Rendus Mathematique*, 354(7):691–696, 2016.

[16] M. Campos Pinto. Structure-preserving conforming and nonconforming discretizations of mixed problems. *hal.archives-ouvertes.fr*, February 2017.

[17] M. Campos Pinto, S. Jund, S. Salmon, and E. Sonnendrücker. Charge conserving FEM-PIC schemes on general grids. *C.R. Mecanique*, 342(10-11):570–582, 2014.

[18] M. Campos Pinto, M. Lutz, and M. Mounier. Electromagnetic PIC simulations with smooth particles: a numerical study. *ESAIM: Proc.*, 53:133–148, 2016.

[19] M. Campos Pinto, M. Mounier, and E. Sonnendrücker. Handling the divergence constraints in maxwell and vlasov–maxwell simulations. *Applied Mathematics and Computation*, 272:403–419, 2016.

[20] M. Campos Pinto and E. Sonnendrücker. Compatible Maxwell solvers with particles I: conforming and non-conforming 2D schemes with a strong Ampère law. HAL preprint, ⟨hal-01303852v1⟩, 2016.

[21] M. Campos Pinto and E. Sonnendrücker. Compatible Maxwell solvers with particles II: conforming and non-conforming 2D schemes with a strong Faraday law. HAL preprint ⟨hal-01303861⟩, 2016.

[22] M. Campos Pinto and E. Sonnendrücker. Gauss-compatible Galerkin schemes for time-dependent Maxwell equations. *Mathematics of Computation*, 2016.

[23] M. Cessenat. *Mathematical methods in electromagnetism*, volume 41 of *Series on Advances in Mathematics for Applied Sciences*. World Scientific Publishing Co., Inc., River Edge, NJ, 1996.

[24] S.H. Christiansen. Stability of Hodge decompositions in finite element spaces of differential forms in arbitrary dimension. *Numerische Mathematik*, 107(1):87–106, 2007.

[25] S.H. Christiansen and R. Winther. Smoothed projections in finite element exterior calculus. *Mathematics of Computation*, 77(262):813–829, 2008.

[26] A. Crestetto and Ph. Helluy. Resolution of the Vlasov-Maxwell system by PIC Discontinuous Galerkin method on GPU with OpenCL. *ESAIM: Proceedings*, 38:257–274, 2012.

[27] L. Demkowicz. Polynomial exact sequences and projection-based interpolation with application to maxwell equations. In *Mixed finite elements, compatibility conditions, and applications*, pages 101–158. Springer, 2008.

[28] L. Demkowicz and A. Buffa. H^1, $H(\mathrm{curl})$ and $H(\mathrm{div})$-conforming projection-based interpolation in three dimensions: Quasi-optimal p-interpolation estimates. *Computer Methods in Applied Mechanics and Engineering*, 194(2):267–296, 2005.

[29] S. Depeyre and D. Issautier. A new constrained formulation of the Maxwell system. *Rairo-Mathematical Modelling and Numerical Analysis-Modelisation Mathematique Et Analyse Numerique*, 31(3):327–357, 1997.

[30] J.W. Eastwood. The virtual particle electromagnetic particle-mesh method. *Computer Physics Communications*, 64(2):252–266, 1991.

[31] A. Ern and J.-L. Guermond. Finite Element Quasi-Interpolation and Best Approximation . ⟨hal-01155412v2⟩, 2015.

[32] T.Z. Esirkepov. Exact charge conservation scheme for Particle-in-Cell simulation with an arbitrary form-factor. *Computer Physics Communications*, 135(2):144–153, 2001.

[33] R. Falk and R. Winther. Local bounded cochain projections. *Mathematics of Computation*, 83(290):2631–2656, 2014.

[34] L. Fezoui, S. Lanteri, S. Lohrengel, and S. Piperno. Convergence and stability of a discontinuous Galerkin time-domain method for the 3D heterogeneous Maxwell equations on unstructured meshes. *ESAIM: Mathematical Modelling and Numerical Analysis*, 39(6):1149–1176, November 2005.

[35] V. Girault and P.-A. Raviart. *Finite Element Methods for Navier-Stokes Equations – Theory and Algorithms*. Springer Series in Computational Mathematics. Springer-Verlag, Berlin, 1986.

[36] E. Gjonaj, T. Lau, and T. Weiland. Conservation Properties of the Discontinuous Galerkin Method for Maxwell Equations. In *2007 International Conference on Electromagnetics in Advanced Applications*, pages 356–359. IEEE, 2007.

[37] J.S. Hesthaven and T. Warburton. Nodal High-Order Methods on Unstructured Grids. *Journal of Computational Physics*, 181(1):186–221, 2002.

[38] J.S. Hesthaven and T. Warburton. High-order nodal discontinuous Galerkin methods for the Maxwell eigenvalue problem. *Philosophical Transactions of the Royal Society A: Mathematical, Physical and Engineering Sciences*, 362(1816):493–524, March 2004.

[39] R. Hiptmair. Canonical construction of finite elements. *Mathematics of Computation*, 68(228):1325–1346, 1999.

[40] R. Hiptmair. Finite elements in computational electromagnetism. *Acta Numerica*, 11:237–339, 2002.

[41] R. Hiptmair. Maxwell's Equations: Continuous and Discrete. In A Bermúdez de Castro and A Valli, editors, *Computational Electromagnetism, Lecture Notes in Math., Vol. 2148*, pages 1–58. Springer International Publishing, Switzerland, 2015.

[42] D. Issautier, F. Poupaud, J.-P. Cioni, and L. Fezoui. A 2-D Vlasov-Maxwell solver on unstructured meshes. In *Third international conference on mathematical and numerical aspects of wave propagation*, pages 355–371, 1995.

[43] G.B. Jacobs and J.S. Hesthaven. High-order nodal discontinuous Galerkin particle-in-cell method on unstructured grids. *Journal of Computational Physics*, 214(1):96–121, May 2006.

[44] G.B. Jacobs and J.S. Hesthaven. Implicit–explicit time integration of a high-order particle-in-cell method with hyperbolic divergence cleaning. *Computer Physics Communications*, 180(10):1760–1767, October 2009.

[45] P. Joly. Variational methods for time-dependent wave propagation problems. In *Topics in computational wave propagation*, volume 31 of *Lect. Notes Comput. Sci. Eng.*, pages 201–264. Springer, Berlin, 2003.

[46] M. Kraus, K. Kormann, P.J Morrison, and E. Sonnendrücker. Gempic: Geometric electromagnetic particle-in-cell methods. *arXiv preprint arXiv:1609.03053*, 2016.

[47] A.B. Langdon. On enforcing Gauss' law in electromagnetic particle-in-cell codes. *Comput. Phys. Comm.*, 70:447–450, 1992.

[48] T. Lau, E. Gjonaj, and T. Weiland. The Construction of Discrete Gauss Laws for Time Domain Schemes. *Magnetics, IEEE Transactions on*, 44(6):1294–1297, 2008.

[49] R. Leis. *Initial-boundary value problems in mathematical physics*. B. G. Teubner, Stuttgart; John Wiley & Sons, Ltd., Chichester, 1986.

[50] C.G. Makridakis and P. Monk. Time-discrete finite element schemes for Maxwell's equations. *RAIRO Modél Math Anal Numér*, 29(2):171–197, 1995.

[51] B. Marder. A method for incorporating Gauss's law into electromagnetic PIC codes. *J. Comput. Phys.*, 68:48–55, 1987.

[52] P. Monk. A mixed method for approximating Maxwell's equations. *SIAM Journal on Numerical Analysis*, pages 1610–1634, 1991.

[53] P. Monk. Analysis of a Finite Element Method for Maxwell's Equations. *SIAM Journal on Numerical Analysis*, 29(3):714–729, June 1992.

[54] P. Monk. An analysis of Nédélec's method for the spatial discretization of Maxwell's equations. *Journal of Computational and Applied Mathematics*, 47(1):101–121, 1993.

[55] P. Monk. *Finite Element Methods for Maxwell's Equations*. Numerical Mathematics and Scientific Computation. Oxford University Press, New York, University of Delaware, Newark, 2003.

[56] P. Monk and L Demkowicz. Discrete compactness and the approximation of Maxwell's equations in R3. *Mathematics of Computation*, 70:507–523, 2001.

[57] H. Moon, F.L. Teixeira, and Y.A. Omelchenko. Exact charge-conserving scatter–gather algorithm for particle-in-cell simulations on unstructured grids: A geometric perspective. *Computer Physics Communications*, 194:43–53, 2015.

[58] C.-D. Munz, P. Omnes, R. Schneider, E. Sonnendrücker, and U. Voß. Divergence Correction Techniques for Maxwell Solvers Based on a Hyperbolic Model. *Journal of Computational Physics*, 161(2):484–511, July 2000.

[59] C.-D. Munz, R. Schneider, E. Sonnendrücker, and U. Voß. Maxwell's equations when the charge conservation is not satisfied. *Comptes Rendus de l'Académie des Sciences-Series I-Mathematics*, 328(5):431–436, 1999.

[60] D.-Y. Na, Y.A. Omelchenko, H. Moon, B.-H. Borges, and F.L. Teixeira. Axisymmetric Charge-Conservative Electromagnetic Particle Simulation Algorithm on Unstructured Grids: Application to Vacuum Electronic Devices. *arXiv:1112.1859v1 [math.NA]*, January 2017.

[61] J.-C. Nédélec. Mixed finite elements in $\mathbf{R^3}$. *Numerische Mathematik*, 35(3):315–341, 1980.

[62] A. Pazy. *Semigroups of linear operators and applications to partial differential equations*. Springer-Verlag, New York, 1983.

[63] P.-A. Raviart and J.-M. Thomas. A mixed finite element method for 2nd order elliptic problems. In *Mathematical aspects of finite element methods, Lecture Notes in Math., Vol. 606*, pages 292–315. Springer, Berlin, 1977.

[64] R.N. Rieben, G.H. Rodrigue, and D.A. White. A high order mixed vector finite element method for solving the time dependent Maxwell equations on unstructured grids. *Journal of Computational Physics*, 204(2):490–519, April 2005.

[65] J. Schöberl. A posteriori error estimates for Maxwell equations. *Mathematics of Computation*, 77(262):633–649, 2008.

[66] J. Squire, H. Qin, and W.M. Tang. Geometric integration of the Vlasov-Maxwell system with a variational particle-in-cell scheme. *Physics of Plasmas (1994-present)*, 19(8):084501, August 2012.

[67] A. Stock, J. Neudorfer, M. Riedlinger, G. Pirrung, G. Gassner, R. Schneider, S. Roller, and C.-D. Munz. Three-Dimensional Numerical Simulation of a 30-GHz Gyrotron Resonator With an Explicit High-Order Discontinuous-Galerkin-Based Parallel Particle-In-Cell Method. *IEEE Transactions on Plasma Science*, 40(7):1860–1870, July 2012.

[68] A. Stock, J. Neudorfer, R. Schneider, C. Altmann, and C.-D. Munz. Investigation of the Purely Hyperbolic Maxwell System for Divergence Cleaning in Discontinuous Galerkin based Particle-In-Cell Methods. In *COUPLED PROBLEMS 2011 IV International Conference on Computational Methods for Coupled Problems in Science and Engineering*, 2011.

[69] M.L. Stowell and D.A. White. Discretizing Transient Current Densities in the Maxwell Equations. In *ICAP 2009*, 2009.

[70] J. Villasenor and O. Buneman. Rigorous charge conservation for local electromagnetic field solvers. *Computer Physics Communications*, 69(2-3):306–316, 1992.

[71] T. Weiland. Finite Integration Method and Discrete Electromagnetism. In *Computational Electromagnetics*, pages 183–198. Springer Berlin Heidelberg, Berlin, Heidelberg, 2003.

[72] D.A. White, J.M. Koning, and R.N. Rieben. Development and application of compatible discretizations of Maxwell's equations. In *Compatible Spatial Discretizations*, pages 209–234. Springer, New York, 2006.

[73] F.S. Yee. Numerical solution of initial boundary value problems involving maxwell's equations in isotropic media. *IEEE Trans. Antennas Propag.*, 14:302–307, 1966.

[74] K. Yosida. *Functional analysis*, volume 123 of *Classics in Mathematics*. Springer-Verlag, Berlin, sixth edition, 1995.

[75] S. Zaglmayr. *High order finite element methods for electromagnetic field computation*. PhD thesis, Universität Linz, Diss, 2006.

[76] J. Zhao. Analysis of finite element approximation for time-dependent Maxwell problems. *Mathematics of Computation*, 73(247):1089–1106, 2004.